Heliyon 10 (2024) e25867

Contents lists available at ScienceDirect

Heliyon

journal homepage: www.cell.com/heliyon

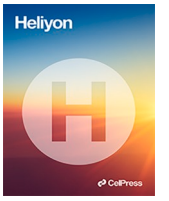

Review article

A review on wear, corrosion, and wear-corrosion synergy of high entropy alloys

Tarik Zirari, Vera Trabadelo *

Mohammed VI Polytechnic University (UM6P), High Throughput Multidisciplinary Research Laboratory (HTMR), Lot 660, Hay Moulay Rachid, 43150, Benguerir, Morocco

ARTICLE INFO

Keywords:
Corrosion
Wear
Erosion
Abrasion
High entropy alloy
Synergy
Tribocorrosion

ABSTRACT

Wear (erosion/abrasion) and corrosion act in synergy in several industrial installations where corrosive fluids circulate together with a solid phase causing mutual damage. High entropy alloys (HEAs) are promising materials to be used in that type of environments because of their outstanding chemical, electrochemical and mechanical properties. While several review articles are currently available on corrosion, mechanical properties, development of HEAs, microstructure, and HEA coatings, there is an undeniable lack of a comprehensive and critical review focusing on the tribological behaviour and tribocorrosion of bulk HEAs. This work aims to collect, summarise, and critically review the major accomplishments and progresses of HEAs over the last 20 years dealing with wear, corrosion, and wear-corrosion resistance. It highlights the most significant aspects that can influence the performance of HEAs including the change of the base alloying elements, the influence of the temperature, heat treatment, and wear test parameters (load, velocity, duration, distance). Furthermore, operating mechanisms, together with the relationship between microstructure and wear resistance, and between microstructure and corrosion resistance will be described. Finally, the articles that have been reported in the literature dealing with tribocorrosion of HEAs will be reviewed. The results of this study are expected to guide potential researchers and provide them with the sum of current trends in HEAs in terms of corrosion resistance, wear resistance and the synergy of both, in the hope of helping them to make the right decision to design and develop new HEAs or improve the research on the existing ones.

1. Introduction

Many risks can be generated because of the action of abrasion, erosion, corrosion, and tribocorrosion, being major threats to the economy, the environment, and the safety of human beings. Corrosion is one of the most critical factors responsible for the degradation of metallic materials used in several industrial processes including gas, automobile, windmill rotors, turbines, and chemical sectors [1]. It is considered as a silent killer of equipment and infrastructures, as its initiation and propagation are beyond the scope of normal visual inspection [2,3]. Wear is responsible for approximately 80% of mechanical moving systems failures [4]; it is defined as the damage of a solid surface caused by the removal or displacement of material, due to the mechanical action of a surface in moving contact. The combined action of wear and corrosion can generate much higher total material losses than the cumulative effects of each

* Corresponding author.
E-mail address: vera.trabadelo@um6p.ma (V. Trabadelo).

https://doi.org/10.1016/j.heliyon.2024.e25867
Received 8 November 2023; Received in revised form 2 February 2024; Accepted 5 February 2024
Available online 11 February 2024

process alone [5,6]. This synergistic combination of wear and corrosion makes corrosion to be accentuated by the breakdown of the passivation films because of wear. On the other hand, erosion/abrasion is influenced by corrosion when small porous particles, such as rust, resulting from oxidation, abrade the surface [7]. Therefore, tribocorrosion, understood as a material degradation resulting from the simultaneous action of wear and corrosion, is an issue of concern for industrial installations in which corrosive fluids circulate together with a solid phase causing a mutual damage [8].

Many industrial facilities experience repeated failures and do not achieve their maximum efficiency because of the lack of high-performant materials capable of withstanding harsh conditions. Nuclear reactor pipes, oil pipelines, and sulfuric and phosphoric acid pumps are among the most affected parts of industrial fluid transport systems [9]. They should be made of appropriate materials to resist mechanical and/or chemical deterioration. Cathodic protection, inhibitors, and microalloying are used to prevent corrosion [10,11]. Tool steels and high-speed steels are used for wear resistance [12,13]. However, few alloys are appropriate for tribocorrosion resistance; it is therefore necessary the development of new alloys to further increase their ability to withstand corrosion and wear simultaneously [14].

For almost a century, there have been no discoveries of new stable metallic elements. This limitation has driven research into what it is called High Entropy Alloys (HEAs); also referred to as Complex Concentrated Alloys (CCA) [9,15]. In the last few years, HEAs have highlighted a new metallurgical paradigm in alloy design, challenging the traditional approach of developing alloys having one major element and minor alloying elements [16]. HEAs are considered as solid solutions that contain more than 5 main elements in equiatomic or near equiatomic proportions with simple crystal structure; they were defined by Yeh et al. [17] and referred as multi-component alloys by Cantor et al. [18–20]. Among the main advantages of HEAs are the opening of a new era of complexity for more degrees of freedom, since there are many alloying systems that can be developed by focusing on the central region of the phase diagram, rather than near the corners (conventional alloys) [9]. HEAs show attractive characteristics regarding wear resistance, mechanical properties, and corrosion resistance (in the range of austenitic and ferritic stainless steels) [21,22].

This work provides a comprehensive overview of the corrosion and wear resistance of HEAs to shed light on the commonalities and the unique differences compared to conventional alloys, when responding to the modification or the influence of the study parameters, such as, content of base alloying chemical elements, temperature, heat treatment, and sliding parameters (load, velocity, duration, distance). Furthermore, operating mechanisms, together with the relationship between microstructure and wear resistance, and between microstructure and corrosion resistance will be described. In the last section, the articles that have been reported in the literature dealing with tribocorrosion (abrasion/erosion-corrosion) of HEAs will be reviewed.

This review intends to be as exhaustive as possible covering the published literature, and it remarks those HEAs whose performance is equal or better than the existing conventional alloys. In addition, this review deals with bulk HEAs, therefore coatings are considered out of its scope.

2. Wear resistance of HEAs

2.1. Effect of the base elements on the wear behaviour

Since the first research article dealing with the wear resistance of HEAs published in 2004 [23], most of the subsequent articles in the field of tribology of HEAs have used the alloy CrFeCoNi as a base system. Several elements have been added to that base alloy, such as aluminium (Al), copper (Cu), titanium (Ti), boron (B), silicon (Si), carbon (C), molybdenum (Mo), manganese (Mn), and so forth, in order to enhance one specific property or a variety of properties (strength, hardness, corrosion resistance, high temperature wear, etc.) [24–26].

Aluminium is considered as the most studied element in HEAs [27–33]. The wear behaviour of Al_xCrFeCoNiCu ($x = 0.5$, 1.0, 1.5, 2.0 in molar ratio) HEAs was investigated by modifying their aluminium content [27]. As the Al content increased from $x = 0.5$ to $x = 2.0$, the hardness increased significantly from 225 HV to 560 HV, respectively, due to the formation of BCC phase. That phase is known by its low plasticity and hard movement of dislocations. As a result, the specific wear rate, which is inversely proportional to hardness, decreased. This special composition of HEAs showed its efficiency to withstand wear under unlubricated conditions.

By replacing copper with titanium and increasing the molar ratio of nickel (Ni) and cobalt (Co) from 1.0 to 1.5 in the Al_xCrFeCoNiCu system, a new HEA is defined as $Al_xCo_{1.5}CrFeNi_{1.5}Ti_y$ where $x = 0$, 0.2 and $y = 0.5$, 1.0 in molar ratio. Four compositions were developed and tested: $CrCo_{1.5}FeNi_{1.5}Ti_{0.5}$ (Al00Ti05), $Al_{0.2}CrCo_{1.5}FeNi_{1.5}Ti_{0.5}$ (Al02Ti05), $CrCo_{1.5}FeNi_{1.5}Ti$ (Al00Ti10), and $Al_{0.2}CrCo_{1.5}FeNi_{1.5}Ti$ (Al02Ti10) [28]. It was observed that the hardness decreased when decreasing the Ti content due to the presence of the brittle FCC γ-phase in the Al00Ti05 and Al02Ti05 alloys. When increasing the amount of Ti, the microstructure showed a coarse η-phase and an Al-rich phase in the interdendritic regions. The former was responsible for the increase in hardness up to 910 HV, whereas the latter phase had a hardness of 1197 HV. The results showed that, although the hardness of Al02Ti10 is similar to that of SUJ2 (AISI 52100) high carbon alloy bearing steel, its wear resistance is 3.6 times higher than that of the conventional alloy. And, although the hardness of Al00Ti10 is lower than that of SKH51 (AISI M2) high speed steel, their wear rates are similar. This may be ascribed to the oxidation resistance and thermal softening resistance of the HEAs.

When adding 0.75 molar ratio of titanium to the CrFeCoNi system already alloyed with Al, the alloy $Al_{0.25}Ti_{0.75}$CoCrFeNi is obtained [29]. Its microstructure consists mainly of 78% of χ phase (matrix) and 20% of a ductile ordered phase (called $L2_1$ phase or Heusler phase). The χ phase is a phase enriched in Co, Cr, and Fe that shows a high value of hardness (1090 HV), while the $L2_1$ phase possesses an FCC lattice and a hardness of 570 HV. It is worth mentioning that the Heusler phase exhibits no obvious splits or cracks compared to the brittle χ phase. The low coefficient of friction of about 0.3, the low wear rate (1.2×10^{-5} $mm^3/N{\cdot}m$), as well as the high hardness of χ and $L2_1$ phases are among the reasons for considering the $Al_{0.25}Ti_{0.75}$CoCrFeNi HEA as a promising alloy for wear

resistance.

The study of the influence of the titanium content on the wear behaviour of the HEA $AlCoCrFeNiTi_x$ ($x = 0$, 0.2, 0.5, 0.8, 1.0, 1.5 in molar ratio) was performed by Löbel et al. [34]. When increasing the Ti content, the microhardness increased from 550 HV for $x = 0$ to 770 HV for $x = 1.0$. This increase in hardness was in accordance with the phases detected. The formation of the BCC phase took place for $AlCoCrFeNiTi_x$ ($x = 0$) HEA (ordered BCC with B2 structure and disordered BCC with A2 structure). When the Ti content increased, additional phases were formed, such as FCC (especially for $x \geq 0.5$) and other complex phases (tetragonal and hexagonal Laves phase). These complex phases should be prevented from occurring in order to achieve high wear resistance and avoid brittleness. All the investigated samples showed higher wear resistance than AISI 5210.

When adding silicon to the CrFeCoNi system already alloyed with Al, the microstructure transforms from BCC + FCC to BCC + Cr_3Si; this fact is responsible for the increase in microhardness from 500 to 908 HV, respectively. Furthermore, $AlCrFeCoNiSi_x$ ($x = 0$, 0.5, 1.0, 1.5, 2.0 in molar ratio) HEAs show better wear resistance as the amount of Si increases from $x = 0$ to $x = 2.0$ [30].

When adding 0.25 mole of Al and 0.6 mole of Si to the CrFeCoNi system, the microstructure of the resulting $Al_{0.25}CoCrFeNiSi_{0.6}$ HEA consists of a mixture of FCC + BCC solid solution phases and needle-shape Cr_3Si intermetallic phase responsible for the increase of microhardness (710 HV) and the decrease of wear rate (3.1×10^{-5} $mm^3N^{-1}m^{-1}$) [31]. Therefore, this HEA is considered as a promising wear resistant material having low aluminium content.

Jin et al. [32] changed the aluminium content while keeping the silicon content constant (1 M ratio of Si). As the aluminium content increased, the microstructure of $Al_xCrFeCoNiSi$ ($x = 0.5$, 1.0, 1.5, 2.0 in molar ratio) HEA went from BCC + FCC + Cr_3Si to BCC + Cr_3Si. Accordingly, the microhardness increased from 598 HV for $x = 0$ to 909 HV for $x = 2.0$ due to the formation of BCC phase. As a result, $Al_xCrFeCoNiSi$ showed low friction, low mass loss, and thus excellent wear resistance due to the strengthening mechanism.

Eutectic high entropy alloys (EHEAs), first proposed by Lu et al. [35], have attracted significant attention due to their exceptional properties. Among those reported outstanding properties there are the combined effect of strength and plasticity, wear resistance, creep resistance at elevated temperatures, and good corrosion resistance for numerous industrial applications (nuclear reactors, gas turbines and aeronautics) [36]. Eutectic forming elements are defined as the elements added to high entropy-based systems having chromium, iron, cobalt and nickel, to form eutectic high entropy alloys. Those elements are aluminium, niobium (Nb), tantalum (Ta), zirconium (Zr), and hafnium (Hf) [37]. They are supposed to turn the original single phase into eutectic microstructures. This is mainly attributed to the large difference in mixing enthalpies between the high entropy-based elements and the eutectic forming elements [38]. Gwalani et al. [33] investigated the influence of B2 precipitates on the wear resistance of the hypoeutectic $Al_{0.5}CoCrFeNi$ HEA by adding 0.5 mole of Al to the CrFeCoNi system. The produced alloy was first hot rolled, followed by annealing, and then isothermally aged at 700 °C. The microstructure, hardness, and wear resistance were determined as a function of the aging time (1, 4, 20, 40, 80 h). $Al_{0.5}CoCrFeNi$ showed heterogeneous and high strength precipitates of B2 phase responsible for improving the mechanical properties. Three types of B2 phase were observed in the alloy: interdendritic B2-phase formed during solidification, solid precipitates, and needle shaped precipitates. Their precipitation increased with aging time, which led to an increase in hardness and therefore in wear resistance, as seen in Table 1.

In 2004, Hsu et al. [23] added boron to the $Al_{0.5}CrFeCoNiCu$ HEA. The as-cast microstructure was composed of dendritic and interdendritic regions, which was confirmed by Wu et al. [27] who eventually found that the microstructure consisted of dendrites and Cu-rich interdendritic regions having brittle FCC phase. By adding between $x = 0$ and $x = 1.0$ mole of B to the $Al_{0.5}CrFeCoNiCu$ HEA, iron and chromium borides were detected in the form of strings, and the size of the precipitates increased as the amount of B increased. Those precipitates were responsible for the high hardness, and therefore high wear resistance of the alloy. Compared to SUJ2 and SKD61 (AISI H13) tool steel, $Al_{0.5}CrFeCoNiCuB$ has low wear rates and can consequently be used for the manufacture of tools and moulds at low or even high temperatures [23].

On the other hand, adding up to 1.2 M ratio of vanadium to the $Al_{0.5}CrFeCoNiCu$ HEA enhanced hardness and wear resistance. In fact, the wear rate increased when the V molar ratio value was between $x = 0.6$ and $x = 1.2$, and the highest value of hardness was measured when $x = 1.0$. By combining these two results, the optimum wear resistance is found when the V content ranges between $x = 1.0$ and $x = 1.2$. This may be attributed to the transformation of FCC phase in the as-cast HEA to BCC+σ-phase [39].

In 2010, Hsu et al. [40] studied the effect of the iron content on the wear behaviour of $AlCrFe_xCoNiMo_{0.5}$ ($x = 0.6$, 1.0, 1.5, 2.0 in molar ratio) HEA derived from the AlCrFeCoNiCu system by changing copper with molybdenum. The microstructure consisted of BCC solid solution and σ-phase. When adding between $x = 0.6$ and $x = 1.0$ mole of Fe, the microstructure showed dendrites richer in aluminium and nickel, and interdendritic regions richer in molybdenum and chromium. The polygrain structure appeared when adding between $x = 1.5$ and $x = 2.0$ of Fe. As the amount of Fe increased, the BCC phase increased at the expense of the σ-phase. Consequently, the total hardness started to decrease, since the hardness of the BCC phase is lower than that of σ-phase. As a result, the

Table 1
Hardness and wear for $Al_{0.5}CoCrFeNi$ hot rolled and annealed (HRA) with and without hold times. Reproduced with permission from Ref. [33].

Condition	Hardness (HV)	Track width (mm)	Wear rate ($10^{-5}mm^3/N{\cdot}m$)
HRA	250.6 ± 6.5	0.93	11 ± 1.4
HRA-700 °C/1 h	258.2 ± 9.9	0.59	4.9 ± 0.9
HRA-700 °C/4 h	254.5 ± 9.5	0.56	5.8 ± 1.5
HRA-700 °C/20 h	296.4 ± 11	0.54	5.4 ± 0.8
HRA-700 °C/40 h	283.5 ± 7.6	0.37	2.7 ± 0.2
HRA-700 °C/80 h	302.2 ± 14.5	0.36	1.8 ± 0.2

wear rate increased when the Fe content increased. Furthermore, the oxidation rate increased when increasing the Fe content, leading to the appearance of more oxides which had the ability to abrade the alloy surface.

It is well known that carbon is one of the most important alloying elements in steels for wear resistance because of its tendency to precipitate hard carbides. This method can be also suitable for HEAs to generate harder compositions. Xiao et al. [41] investigated the effect of carbon content on the wear resistance of C_xCrFeCoNiMn HEAs with different compositions ($x = 0$, 0.3, 0.6, 0.9, 1.2 in molar ratio). The microstructure of the studied HEAs consisted of FCC phase structure rich in cobalt and nickel together with M_7C_3 carbides richer in chromium. The quantity of these carbides increased when increasing the carbon content, and this fact improved the scratch resistance and reduced the wear rate of the alloys having x below 0.6. When $x = 0.6$, $C_{0.6}$CrFeCoNiMn HEA is considered as the optimal composition with the lowest coefficient of friction, highest hardness and scratch resistance, and thus highest wear resistance. That is why, for that alloy, the scratch grooves are the shallowest (Fig. 1a) and the scratch volume shows the lowest value (Fig. 1b). However, these parameters drop gradually when the amount of C is greater than $x = 0.6$. This is arguably attributed to the increase in porosity of M_7C_3 carbides, which goes from 1.7% when $x = 0.6$ to 8.7% when $x = 1.2$.

2.2. Wear mechanisms

As shown in Section 2.1, modifying the base elements content of the HEAs has a great influence on the wear mechanism. By adding Al, the wear mechanism of Al_xCoCrCuFeNi ($x = 0.5$, 1.0, 2.0 in molar ratio) HEAs changes from adhesive wear, especially delamination wear, to delamination and oxidative wear when the value of Al goes from $x = 0.5$ to $x = 1.0$ [27]. This is mainly due to the nature of the phases that constitute the alloy. In fact, the microstructure of $Al_{0.5}$CoCrCuFeNi consists of FCC brittle phase which undergoes delamination wear, whereas $Al_{1.0}$CoCrCuFeNi consists of FCC and hard BCC phases. In this latter composition, the O_2 content of the worn surfaces increases, and thus the oxidative wear is becoming noticeably marked. When the Al content reaches $x = 2.0$, the mechanism thoroughly transforms to oxidative wear noticed by the higher O_2 concentration in the wear debris, and the resistance to delamination owing to the BCC phase.

On the contrary, although the worn surfaces of AlCoCrFeNiSi$_x$ ($x = 0$, 0.5, 1.0, 1.5, 2.0), AlCoCrFe$_x$Mo$_{0.5}$Ni ($x = 0.6$, 1.0, 1.5, 2.0), and Al_xCrFeCoNiSi ($x = 0.5$, 1.0, 1.5, 2.0) HEAs exhibit trace amounts of O_2, the wear mechanism is predominantly abrasive, rendering hard oxide debris [30,32,40]. The worn surfaces are always showing grooves, and thus abrasive wear is occurring in all cases. The carbon-free CrFeCoNiMnC_x ($x = 0$, 0.3, 0.6, 0.9, 1.2) has a significantly rough surface due to the soft and brittle FCC phase. The initiation of pits can be observed in regions where the debris is peeled off, and thus, the mechanism is mainly delamination wear [41]. When adding 0.6 mole of carbon to the CrFeCoNiMn HEA, the delamination wear is no longer detected. The decreased degradation of the worn surface may be explained by the precipitation of M_7C_3 carbides responsible for the excellent wear resistance of CrFeCoNiMn$C_{0.6}$. As the amount of carbon increases up to 1.2, long and deep grooves and micro-cracks are observed indicating abrasive wear mechanism.

2.3. Effect of the heat treatment

Heat treatments are undoubtedly useful in reducing defects, stresses, cracks, or even the wear rate and in producing alloys with a uniform structure. For instance, Kong et al. [42] investigated the effect of remelting and annealing (without remelting) on the wear resistance of AlCrFeCoNiTi$_{0.5}$. The results showed that the hardness (Fig. 2a), the coefficient of friction, and the wear mass loss (Fig. 2b) were improved significantly for both, remelted and annealed samples, compared to the as-cast HEAs. Furthermore, the annealed samples showed higher wear resistance than the remelted ones.

Superheating (over heating above the melting temperature during the fabrication of the alloy) can be also an effective way to enhance the wear resistance of HEAs. Recently, Kong et al. [45] studied the improvement in wear resistance of $Al_{1.8}$CrCuFeNi$_2$ after melting at different superheating temperatures, (1320 °C, 1360 °C, and 1400 °C) followed by water-cooling. Superheating makes the dendrites grow in a large-angle direction, improving wear resistance. In fact, the best wear resistance was achieved when the

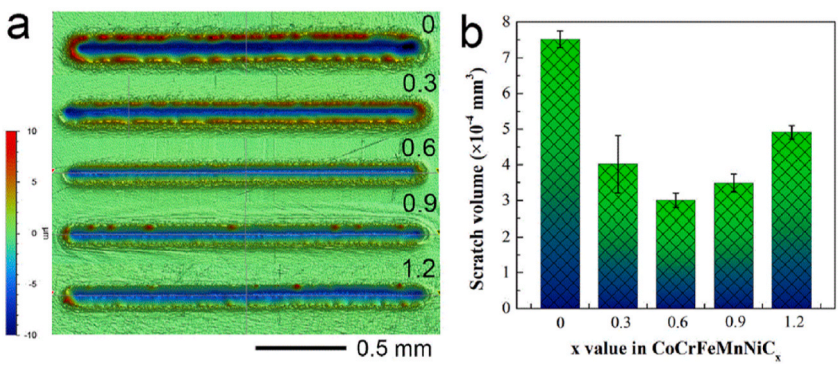

Fig. 1. Scratch resistance of C_xCrFeCoNiMn HEAs: a) 3D images of scratch grooves, and b) scratch volumes. Reproduced with permission from Ref. [41].

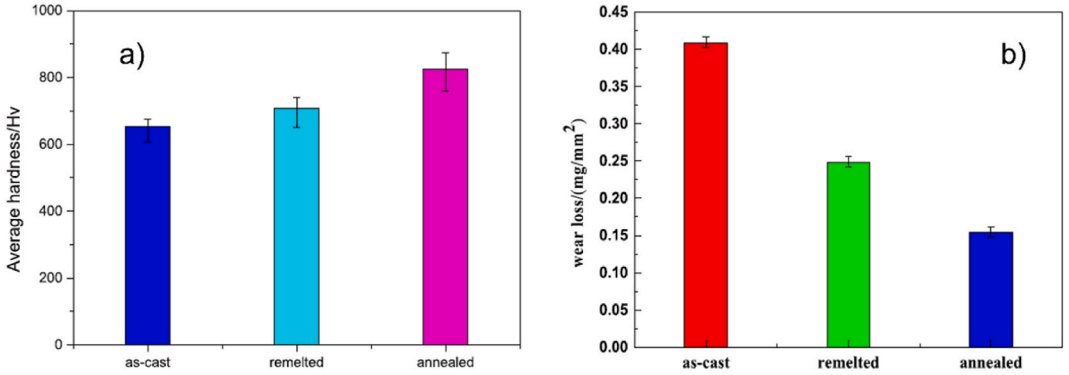

Fig. 2. a) Vickers hardness and b) Wear mass loss of as-cast, remelted and annealed AlFeCrCoNiTi$_{0.5}$ HEA. Reproduced with permission from Ref. [42].

superheating temperature reached 1400 °C.

A recent study performed by Guo et al. [47] showed the effect of heat treatment on the hardness and wear behaviour of AlCoCrFeNiSi HEA. This alloy was subjected to different heat treatments at 1100 °C, 1150 °C, 1185 °C and 1200 °C, and kept for 2 h with air cooling. When the heat treatment temperature exceeded 1150 °C, the BCC interdendritic region narrowed and the dendrite phase disappeared. Furthermore, the precipitated Cr_3Si phase turned into long needle-like microstructure. Although the microhardness of the as-cast HEA was already high (849 HV), the microhardness after heat treatment increased significantly reaching 953.5 and 1004.3 HV, at 1100 °C and 1150 °C respectively; this is due to the homogeneous microstructure and dispersion strengthening. The treated HEA exhibited the lowest friction coefficient (0.115) which is 3.4 times better than that of the as-cast HEA. As a result, the effect of the heat treatment was found to be highly significant in improving the wear resistance.

2.4. Effect of the wear testing conditions

2.4.1. Effect of the testing temperature

The tribological behaviour of $Al_{0.6}$CoCrFeNi [43] was investigated at different temperatures. In this study, the HEA was prepared by arc-melting, then subjected to cold rolling at room temperature followed by annealing at 850 °C for 4 h. It was found that the microstructure of the as-cast $Al_{0.6}$CrFeCoNi consisted of an FCC matrix and BCC phase which had disordered A2 and ordered B2 structures as a direct consequence of spinodal decomposition. After the heat treatment, the annealed $Al_{0.6}$CrFeCoNi comprised FCC phase, B2 and σ-CrFe phases; the volume fraction as well as the size of the FCC and σ-CrFe phases increased considerably. The presence of a hard and brittle σ-CrFe phase markedly improved the hardness, going from 270 HV for the as-cast state to 480 HV for the annealed alloy. The coefficient of friction of the annealed alloy as a function of the sliding time exhibited small fluctuations and decreased as the testing temperature increased. This fact was attributed to the formation of oxide layers and the annihilation of adhesive forces, since they are sensitive to high temperatures. As seen in Fig. 3, up to 100 °C the specific wear rate of the annealed HEA is slightly higher than that of the commercial alloy GCr15 (AISI 52100) bearing steel. As the temperature increases, the wear rate of the annealed HEA remains almost constant between 400 °C and 600 °C and it is about 2.5 times lower than that of GCr15.

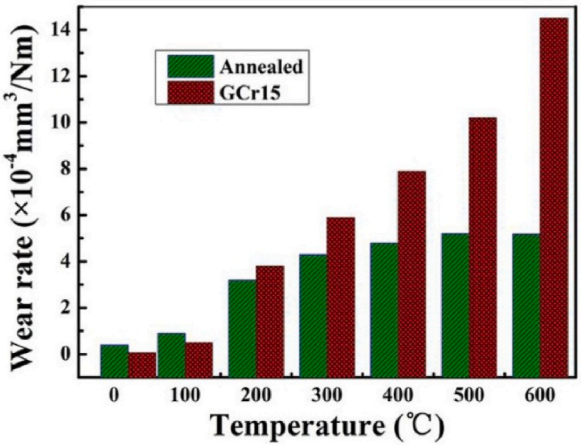

Fig. 3. Wear resistance of $Al_{0.6}$CoCrFeNi annealed alloy and GCr15 vs. test temperature. Reproduced with permission from Ref. [43].

This is ascribed to the fact that the hot hardness of the commercial alloy drops rapidly between 300 °C and 600 °C because of the decomposition of carbides, which are the responsible for the excellent hardness of GCr15 (710 HV) at room temperature. Whereas the σ-CrFe phase in the annealed $Al_{0.6}$CoCrFeNi is stable at elevated temperatures, and thus it confers an excellent softening resistance.

Similarly, Du et al. [44] investigated the influence of temperature on the wear behaviour of the $Al_{0.25}$CrFeCoNi HEA. After production with arc melting, the samples were subjected to cold rolling to minimize the defects of casting, followed by annealing up to 700 °C for 30 min to eliminate residual stresses. The microstructure did not undergo any phase transformation; the FCC lattice was retained in all processing steps. However, the hardness increased during cold rolling due to strain hardening and decreased during the subsequent annealing. This fact is due to the complete destruction of dislocations and residual stresses responsible for the hardening of the alloy. Fig. 4 depicts the effect of testing temperature on the tribological properties of the rolled-annealed $Al_{0.25}$CrFeCoNi HEA. Fig. 4a shows that the specific wear rate increases significantly from room temperature (20 °C) to 350 °C because of the low thermal softening resistance. Instead of continuing to increase, it remains quite stable at high temperatures. This is due to the formation of hard oxide films which are responsible for the decrease of the friction coefficient to a value of 0.51 at 600 °C, as seen in Fig. 4b.

Nguyen et al. [46] investigated the influence of the temperature in the tribological properties of $Al_{0.4}$CrFeNi$Ti_{0.2}$. The wear and friction properties were studied over a temperature range of 600–950 °C. The microstructure of the as-cast HEA consisted of a dendritic structure based on B2 phase enriched in Ni, Al, and Ti; and an interdendritic structure which had a BCC matrix enriched in Cr and Fe. During the homogenization process, the Ti-rich part from the dendritic phase transformed into FCC phase enriched in Ni and Fe. This transformation was responsible for the slight drop of hardness since the BCC phase is harder than the FCC phase. After evaluation of the tribological properties of $Al_{0.4}$CrFeNi$Ti_{0.2}$, it was found that the frictional sliding and wear resistance are significantly dependent on temperature. As observed in Fig. 5a, spanning from 600 °C to 800 °C, the specific wear rate declines gradually due to the wear debris formed during sliding, which withstand the wear loss. On the other hand, as depicted in Fig. 5b, the coefficient of friction increases progressively due to the presence of debris or oxides from the oxidation of the ordered phases (B2 and BCC) which could be abrasive third-body corpuscles leading to an increase of friction. Above 800 °C up to 950 °C, the abrupt decrease in the coefficient of friction may be attributed to the thick oxide film formed on the tribo-layer at elevated temperatures. However, the specific wear rate increases due to the softening of the alloy at high temperature.

Several high entropy alloys have been designed in the last few years for applications that require elevated temperatures. A new class of HEAs called Refractory High Entropy Alloys (RHEAs) was developed for this purpose in the hope of finding outstanding materials to be applied in turbines, reactors and heat tubes, instead of using superalloys or the commercial refractory alloys already existing in the market. RHEAs are based on refractory elements having high melting point, such as vanadium and tungsten (W). Pole et al. [48] investigated the tribological behaviour of HfTaTiVZr and TaTiVWZr RHEAs using sliding and reciprocating wear tests between 25 °C and 450 °C. Both RHEAs have the lowest coefficient of friction reported to date for RHEAs. The results showed that the wear rate increased at temperatures lower than 150 °C because of the wear debris removal out of the contact area (run-in stage). Between 150 °C and 450 °C, the wear rate started to decrease due to the formation of a thick oxide layer containing ZrO_2, TiO_2, Ta_2O_5, V_2O_5, HfO_2, and WO_3 hard oxides, which acted as a protective layer against wear at high temperatures. Both HfTaTiVZr and TaTiVWZr RHEAs showed inferior wear resistance at room temperature and at 996 °C compared to 304 stainless steel, due to the good strain hardening of the commercial alloy. Nevertheless, at elevated temperatures (between 846 °C and 996 °C), the wear resistance of 304 stainless steel was approximately similar to that of TaTiVWZr but still higher than that of HfTaTiVZr.

Some research studies simultaneously dealt with the change of temperature and the addition of one of the main constituent elements. Verma et al. [49] investigated the influence of copper on the CrFeCoNiCu$_x$ ($x = 0, 0.2, 0.4, 0.6, 0.8, 1.0$ in molar ratio) HEAs at high temperatures up to 600 °C. The results showed that the hardness increased when the Cu content increased. This fact was due to the segregation of copper at the grain boundaries, which restricted the growth of grains, and thus limited their size. The specific wear rate at both room and high temperatures decreased when increasing the amount of copper, especially at 600 °C. At this elevated temperature, the high wear resistance was explained by the formation of glaze copper oxide film which acted as an auto-lubricant.

FCC CrFeCoNiMn and FCC $Al_{0.3}$CrFeCoNi showed the highest wear rates at 25 °C due to the softness and brittleness of the FCC phase [50]. At elevated temperatures, the oxide films that form onto the HEAs improve the wear resistance, which is manifested by the decrease in the coefficient of friction. Above 300 °C the tested HEAs (FCC CrFeCoNiMn and FCC $Al_{0.3}$CrFeCoNi) had higher wear

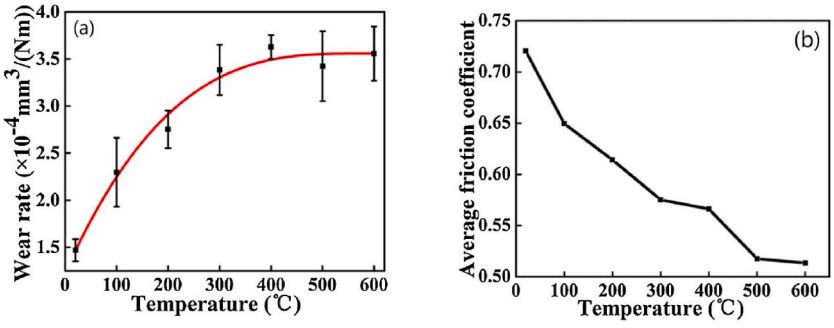

Fig. 4. a) Wear rate of $Al_{0.25}$CrFeCoNi HEA at different test temperatures; b) Variation of its friction coefficient with temperature. Reproduced with permission from Ref. [44].

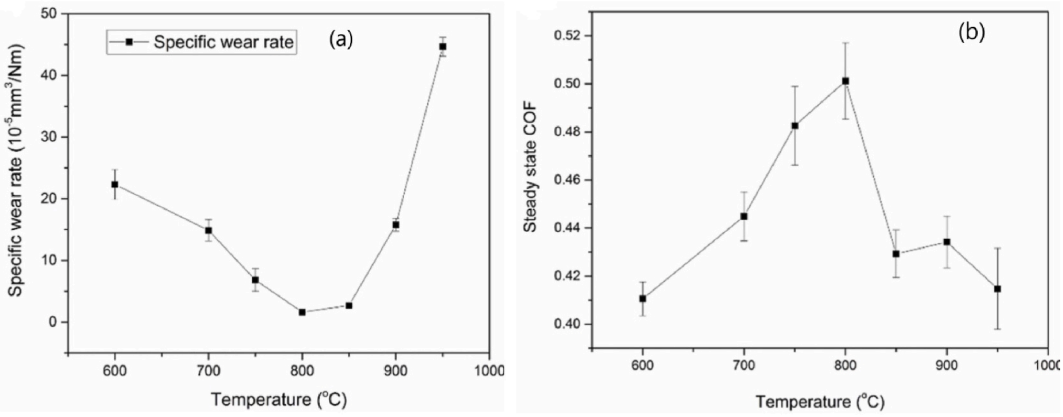

Fig. 5. a) Evolution of specific wear rate as a function of temperature; b) Evolution of the steady-state friction coefficient of $Al_{0.4}CrFeNiTi_{0.2}$ as a function of temperature. Reproduced with permission from Ref. [46].

resistance than the 304 stainless steel, and higher than Inconel 718 above 800 °C. This was mainly attributed to the presence of a protective oxide layer on the worn surface. The high hot-strength (because of σ-phase) and the oxidative wear (because of the Al_2O_3 layer) are the main factors that explain the low wear rate which confers to AlCrFeCoNi an exceptional wear resistance at 900 °C.

The results for the CrFeCoNiMn HEA were implicitly confirmed by Cheng et al. [51] when they investigated the tribological properties of Al_xCrFeCoNiMn ($x = 0$, 0.5, 1.0 in molar ratio) HEAs. Although the experimental procedure was different from that of Joseph et al. [50], the results were relatively similar. The three HEAs possessed improved hot hardness because of the excellent resistance to softening. Furthermore, the wear rate decreased when increasing the Al content, and drastically decreased as the temperature increased, especially beyond 500 °C. The HEAs having high Al content at 800 °C exhibited the lowest coefficient of friction and showed antifriction and wear resistance at the same temperature due to the existence of oxide layers rich in Al. Both studies [50, 51] reported that a nano/ultrafine grained oxide layer formed on the worn surface, preventing the HEA from being damaged by wear during dry sliding friction.

2.4.2. Influence of the sliding distance

Under oil lubricating conditions, the wear resistance and frictional behaviour of the $Al_{0.4}CrFeCo_xNi$ ($x = 0$, 0.25, 0.5, 1.0 in molar ratio) HEAs were studied by modifying the sliding parameters i.e., sliding distance, speed or sliding velocity and normal load [52]. It is worth mentioning that the addition of cobalt does not overlap with the change of sliding test parameters, in any case, they do not have any influence on each other. At a constant sliding speed of 1 m/s and under a normal load of 10 N, the coefficient of friction and the specific wear rate increased as the sliding distance increased. However, at low sliding distance, between 1 km and 2 km, a slight decrease in the coefficient of friction occurred, mainly due to the lubrication stage before the breakage of the lubricating oil film.

2.4.3. Influence of the sliding velocity

According to Kumar et al. [52] the curve depicting the coefficient of friction of $Al_{0.4}CrFeCo_xNi$ ($x = 0$, 0.25, 0.5, 1.0 in molar ratio) as a function of velocity (constant sliding distance of 1000 m and normal load of 10 N) is similar to a Gaussian distribution. When increasing the speed from 1.0 to 1.2 m/s, the increase in the value of the friction coefficient is due to the trapping of worn particles and the breakage of the oil film at the interface between the contacting surfaces. Between 1.2 and 2.0 m/s the enhancement of the coefficient of friction is due to the effectiveness of the tribo-layer at high speeds. The only exception is detected for the cobalt free--$Al_{0.4}CrFeCo_xNi$ HEA, whose coefficient of friction decreases slightly at low speed compared to other compositions. This may be due to the formation of a lubricating oil film. The specific wear rate of the $Al_{0.4}CrFeCo_xNi$ ($x = 0$, 0.25, 0.5, 1.0 in molar ratio) HEAs decreases when increasing the sliding velocity under a normal load of 10 N and a constant sliding distance of 1 km.

Like the previous study [52], the sliding wear behaviour of $Al_{0.4}FeCrNiCo_x$ ($x = 0$, 0.25, 0.5, 1.0 in molar ratio), without lubrication, in dry conditions, was also studied by Kumar et al. [53]. Under a normal load of 10 N and 1 km of sliding distance, the coefficient of friction decreases rapidly, then declines gradually as the sliding velocity increases. This is due to the high contact temperature resulting in the growth of the oxide film, which in turn makes the surface smooth and reduces friction. The specific wear rate acts differently, it does not correlate with the coefficient of friction. The main reason for the decrease in wear resistance is the high temperature at the contacting surface and the absence of lubrication.

Firstov et al. [54] determined the wear mass loss and coefficient of friction for a variety of HEAs as a function of the sliding velocity. After 1 km of sliding distance, FeCoNiCuVMo and $R_{12}M_3F_2K_5$ exhibit the lowest mass loss. On the other hand, Fe–W–CaF_2 shows a significant increase in the mass loss between 10 and 15 m/s. The coefficient of friction decreases when the sliding rate increases, and the FeCoNiCuVMo HEA possesses an excellent coefficient of friction, suggesting that this HEA has the best wear resistance among all the tested materials.

In order to assess the tribological properties of the $CoCrFeNiMo_{0.2}$ HEA at room temperature, dry reciprocating sliding wear tests were performed [55]. The variation of the coefficient of friction was determined as a function of the sliding velocity at a normal load of

20 N and a sliding duration of 600 cycles. Below 60 mm/s, the coefficient of friction showed a non-significant decrease, followed by a rapid decrease as the sliding speed went up to 240 mm/s. The mechanism was explained by the change in the shear rate and surface temperature, which resulted in the change of the mechanical properties. Furthermore, under the same conditions, the specific wear rate was found to have high values at high velocities. This fact was attributed to the formation of tribo-oxide debris.

2.4.4. Influence of the normal load

Under oil lubricating conditions, the coefficient of friction and the specific wear rate of the $Al_{0.4}CrFeCo_xNi$ ($x = 0$, 0.25, 0.5, 1.0 mole) HEAs increase gradually when increasing the normal load from 5 to 20 N. This is due to the increase of the metal-to-metal contact which results in more debris responsible for the surface damage [52]. Similarly, in dry conditions, the coefficient of friction declines gradually in the range of 5–15 N and decreases rapidly after 15 N. The specific wear rate increases rapidly from 5 N to 15 N, then gradually increases from 15 N to 20 N. The increase in the coefficient of friction is due to the fact that the contact surface between the pin and the disc becomes significant under heavy loads. That results in an increase of heat, and therefore promotes the formation of an oxide film responsible for the low coefficient of friction. A second explanation is based on the presence of wear debris, which minimizes the effective contact between the pin and the disc. Al_2O_3, Fe_2O_3, Cr_2O_3, and Co_3O_4 are the oxides formed on the worn surface of $Al_{0.4}CrFeCoNi$.

For the $CoCrFeNiMo_{0.2}$ HEA, the variation of the coefficient of friction was determined as a function of the normal load at a sliding velocity of 6 mm/s and a sliding duration of 600 cycles [55]. Between 5 and 20 N, the coefficient of friction decreased rapidly from 0.719 to 0.627, respectively. As the normal load increased, the coefficient of friction decreased gradually to approximately 0.589 at 80 N (Fig. 6a). In this case, it is not easy to identify the operating mechanism, since it involves several factors, such as thermal softening and oxidation during friction. Using the same sliding conditions, the specific wear rate decreased as the normal load increased (Fig. 6b).

2.4.5. Influence of the environment

The tribological properties of the HEAs are highly dependent on the environment. Therefore, a detailed study in different environments can reveal interesting results on wear characteristics and it can be very useful for applications that require deep understanding of the alloy behaviour in different environments. As reported before [52,53], both studies dealt with the influence of the sliding parameters on the tribological properties of $Al_{0.4}FeCrNiCo_x$ ($x = 0$, 0.25, 0.5, 1.0 molar ratio). However, a comparison between dry sliding medium and lubrication conditions is needed to understand the influence of the environment on the wear resistance of $Al_{0.4}CrFeCo_xNi$. In fact, by increasing the sliding speed, the lubrication contributes to decrease the coefficient of friction to a value below 0.07 and enhance the wear resistance by decreasing the specific wear rate to a value below 2.6×10^{-5} $mm^3/N{\cdot}m$ (compared to dry conditions). When the normal load increases, the coefficient of friction and the specific wear rate increase gradually under lubricated and unlubricated media; however, when increasing the normal load, the coefficient of friction in dry medium slightly declines from 0.3 to 0.225.

Chen et al. [56] investigated the tribological properties of $Al_{0.6}CrFeCoNi$ in dry air, deionized water, simulated acid rain, and seawater at different sliding velocities. This specific HEA was selected owing to its balanced strength and ductility. At high velocities, this HEA exhibited high friction coefficients in ambient air, whereas the values were lower in simulated seawater. The wear rate of the as-cast $Al_{0.6}CrFeCoNi$ in dry conditions was higher than that in wet and corrosive media. Also, the wear rate in deionized water was higher than that in acid rain and seawater because: (1) The lubrication effect was different from one medium to another; (2) The debris might be corroded into more fine particles which, in turn, might polish the surface and form a protective layer against material loss under a normal load.

Liu et al. [57] investigated the tribological properties of the $AlCrCuFeNi_2$ HEA in dry medium, simulated rainwater (pH = 2), and deionized water. It was found that the friction coefficient of this alloy decreases when increasing the normal load. The wear rate is low in deionized water and simulated rainwater compared to that in dry conditions. However, the lowest wear rate was measured in

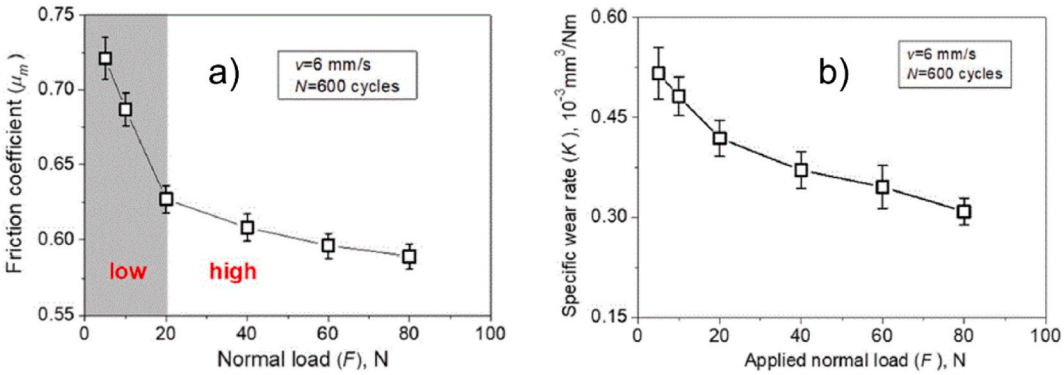

Fig. 6. a) Variation of the friction coefficient of $CoCrFeNiMo_{0.2}$ against the normal load; b) Evolution of the specific wear rate after dry sliding against the normal load. Reproduced with permission from Ref. [55].

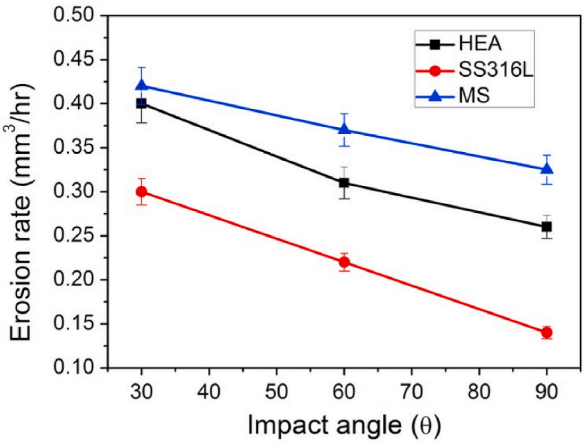

Fig. 7. The cumulative volume loss/hour as the function of impact angle for $Al_{0.1}CrCoFeNi$, 316L stainless steel (SS) and mild steel (MS). Reproduced with permission from Ref. [59].

simulated rainwater under a load of 15 N for which the curves were very smooth with small fluctuations. Under rainwater conditions this HEA exhibits high corrosion resistance compared to the 316L stainless steel. Wet conditions are responsible for the dissipation of heat, since heat build-up increases wear rate considerably, and humidity acts as a lubricant as well. Furthermore, the formation of a protective metallic passive layer improves the wear resistance. By investigating the reciprocating sliding wear behaviour of CoCrFeMnNi and $Al_{0.1}CoCrFeNi$, in dry and marine environments (corrosive medium), it was concluded that $Al_{0.1}CoCrFeNi$ is more wear resistant than CoCrFeMnNi [58]. This may be attributed to the formation of a protective passivation layer in marine environment.

2.4.6. Influence of the impact angle

Nair et al. [59] investigated the slurry erosion behaviour of $Al_{0.1}CrCoFeNi$ in comparison with a mild steel and the 316L stainless steel. The HEA was fabricated using induction melting followed by hot isostatic pressing (HIP). When investigating the slurry erosion as a function of the impingement angle (30°, 60° and 90°) (Fig. 7), it was found that the erosion rate (referred as the corresponding volume loss in 1 h of erosion) of $Al_{0.1}CrFeCoNi$ at an oblique angle (30°), is similar to that of the mild steel (MS) despite the low hardness of the HEA. In general, the erosion rate decreases with the increase of the impact angle.

2.4.7. Influence of the counterpart

HEAs are known by their hardening and strengthening mechanism that makes the hardness of the alloy to be greater than that of its individual constituents. Sliding wear behaviour of the lightweight $CrFeCo_{1.5}Ni_{1.5}Ti_{0.5}$ HEA was investigated when two different counterparts were used, namely, alumina and 100Cr6 steel ball [60]. In both cases, and as one would expect considering the theoretical concepts, the volumetric loss increased with the sliding distance. Unlike 100Cr6 steel ball, the alumina ball caused serious damage on the HEA due to its high hardness. When using the steel ball as a counterpart to investigate the difference in wear resistance between $CrFeCo_{1.5}Ni_{1.5}Ti_{0.5}$ and Inconel 718, it was found that the HEA experienced less wear. Therefore, it could be a potential material in applications where the lightweight criterion and a relatively good wear resistance are required.

Table 2 summarizes the main studies dealing with the wear resistance of HEAs described in section 2.

3. Corrosion resistance of HEAs

3.1. Effect of the base elements on the corrosion behaviour

3.1.1. Effect of Al content

Various studies investigated the influence of the Al content on the corrosion resistance of HEAs. For example, the corrosion behaviour of the $Al_xCrFe_{1.5}Ni_{0.5}Mn$ ($x = 0$, 0.3, 0.5 in molar ratio) HEAs was studied in acid and chloride media [61]. In 0.5 M H_2SO_4 solution, the corrosion resistance of the alloy declined significantly when the content of aluminium increased from $x = 0$ to $x = 0.5$. Thus, the aluminium-free HEA exhibited excellent general corrosion resistance, better than the 304 stainless steel. In chloride media, the addition of aluminium fostered the pitting corrosion, since the potentiodynamic curve in this case indicated lower pitting potentials for the aluminium-free $CrFe_{1.5}Ni_{0.5}Mn$ HEA. In acid environments containing chloride ions, the intensity of pitting corrosion increased with the addition of Al, while the pits become fewer and narrower on the surface of the Al-free $CrFe_{1.5}Ni_{0.5}Mn$.

Accordingly, anodic treatment in 15% H_2SO_4 was used to improve the localized (pitting) corrosion. The anodized $Al_{0.3}CrFe_{1.5}Ni_{0.5}Mn$ showed higher corrosion resistance than the un-anodized alloys [62]. On the other hand, the addition of Al increased the chromium-depleted zone in the $Al_xCoCrFeNi$ (x = 0.3, 0.5, 0.7 in molar ratio) HEAs, which led to localized corrosion [63]. The addition of Al had a drastic impact on the microstructure of the $Al_xCoCrFeNi$ ($x = 0.3$, 0.5, 0.7 molar ratio) HEAs [64]. By increasing the Al content, the microstructure evolved from FCC single phase (A1 phase) for $Al_{0.3}CoCrFeNi$, to a mixture of A1 phase, disordered BCC (A2

Table 2
Summary of the investigations on wear resistance of HEAs.

Alloy composition	Alloy Preparation	Influencing parameter	Hardness (HV)	Coefficient of friction	Wear test conditions	Specific wear rate ($mm^3/N/m$) or Wear rate (mm^3/m) or Erosion rate (mm^3/h) or Wear resistance (m/mm^3)	Wear mechanism	Ref.
$CuCoNiCrAl_{0.5}FeB_x$ ($x = 0, 1.0$)	*Induction melting in air	Effect of boron	$x = 0$: 300 HV $x = 0.2$: 420 HV $x = 0.6$: 500 HV $x = 1.0$: 730 HV	/	*Sliding velocity: 0.5 m/s *Load: 29.4 N (3 kgf) *Sliding distance: 20 m	Wear resistance: $x = 0$: 1.0 $x = 0.2$: 1.04 $x = 0.6$: 1.2 $x = 1.0$: 1.76	/	[23]
$Al_xCoCrCuFeNi$ ($x = 0.5, 1.0, 2.0$)	*Arc melting and casting method *Polishing → etching with aqua regia (HNO_3:HCl = 1:3).	Effect of aluminium	$x = 0.5$: 225 HV $x = 1.0$: 355 HV $x = 2.0$: 560 HV	$x = 0.5$: 0.50 $x = 1.0$: 0.48 $x = 2.0$: 0.32	Sliding wear: *Sliding velocity: 0.5 m/s *Load: 29.4 N *Sliding distance: 20 m * Medium: unlubricated	Specific wear rate: $x = 0.5$: 8.82×10^{-4} $x = 1.0$: 7.26×10^{-4} $x = 2.0$: 4.91×10^{-4}	$x = 0.5$: Delamination $x = 1.0$: Delamination in FCC regions, Oxidative in BCC $x = 2.0$: Oxidative	[27]
$Al_{0.5}CoCrCuFeNiV_x$ ($x = 0, 0.4, 0.6, 1.0, 1.2, 1.4, 1.6, 1.8, 2.0$)	*Arc melting and casting method * Polishing → etching with aqua regia (HNO_3:HCl = 1:3).	Effect of vanadium	$x = 0$: 225 HV $x = 1$: 640 HV $x = 1.2$–2: 590 HV (average)	/	Sliding wear: *Sliding velocity: 0.5 m/s *Load: 29.4 N *Sliding distance: 20 m * Medium: unlubricated	Wear rate: $x = 0.2$: 1.092×10^{-3} $x = 1$: 1.06×10^{-3} $x = 1.2$: 0.94×10^{-3} $x = 2$: 0.88×10^{-3}	/	[39]
$AlCoCrFe_xMo_{0.5}Ni$ ($x = 0.6, 1.0, 1.5, 2.0$)	*Arc melting and casting method	Effect of iron	$x = 0.6$–1.0: 725 HV $x = 1.5$–2.0: 640 HV	0.74	Sliding wear: *Sliding velocity: 0.5 m/s *Sliding time: 24 h *Load: 29.4 N	Wear rate: $x = 0.6$: 7.14×10^{-4} $x = 1.0$: 6.89×10^{-4} $x = 1.5$: 11.76×10^{-4} $x = 2.0$: 22.47×10^{-4}	$x = 2$: Abrasion wear	[40]
$Al_xCo_{1.5}CrFeNi_{1.5}Ti_y$ Comparison with (SUJ2 and SKH51 high speed steel) ($x = 0, 0.2$) and ($y = 0.5, 1.0$)	*Arc-melting * Homogenization at 1100 °C for 4 h in air + air cooling *Aging at 800 °C for 10 h in air + air cooling.	Effect of aluminium and titanium content	$x = 0$, y = 0.5: 509 HV $x = 0$, y = 1.0: 654 HV $x = 0.2$, y = 0.5: 487 HV $x = 0.2$, $y = 1.0$: 717 HV SKH51: 890 HV SUJ2: 722 HV	/	Sliding wear: *Sliding velocity: 0.5 m/s *Load: 29.4 N *Sliding distance: 5.4 Km for $x = 0$, $y = 0.5$ and $x = 0.2$, $y = 0.5$, 4.3 Km for the rest	Wear rate: $x = 0$, $y = 0.5$: 57.14×10^{-4} $x = 0.2$, $y = 0.5$: 50×10^{-4} $x = 0$, $y = 1.0$: 3.63×10^{-4} $x = 0.2$, $y = 1.0$: 1.81×10^{-4} SKH51: 3.63×10^{-4} SUJ2: 6.66×10^{-4}	/	[28]
$Al_{0.1}CrCoFeNi$ (comparison with 316L SS and mild steel)	*Induction melting → hot isostatic pressing (HIP) at 1200 °C for 4 h under 100 MPa → cooling *Grinding (2000 grit size) → Polishing.	Effect of the impingement angle	*$Al_{0.1}CrCoFeNi$: 150 HV *316L SS: 226 HV *Mild steel: 205 HV	/	Slurry erosion: *Velocity: 20 m/s *Temperature: 25 °C *Angle: 30°, 60°, 90° *Particle size: 75–150 mm	Erosion rate: *HEA: At 30°: 0.400 at 60°: 0.310 at 90°: 0.265 *Mild steel: At 30°: 0.425 At 60°: 0.375 At 90°: 0.330	/	[59]

(*continued on next page*)

Table 2 (*continued*)

Alloy composition	Alloy Preparation	Influencing parameter	Hardness (HV)	Coefficient of friction	Wear test conditions	Specific wear rate ($mm^3/N/m$) or Wear rate (mm^3/m) or Erosion rate (mm^3/h) or Wear resistance (m/mm^3)	Wear mechanism	Ref.
$Co_{1.5}CrFeNi_{1.5}Ti_{0.5}$ (comparison with AISI H13 and Inconel 718)	*Arc melting → re-melting (x5) for homogeneous distribution of the elements	Effect of the counterpart	368 HV	/	Sliding wear *Sliding velocity: 0.1 m/s *Load: 5 N *Sliding distance: 1 Km	Wear rate: *Al_2O_3 as a counterpart: HEA: 1.13×10^{-3} *Steel ball counterpart: HEA: 0.52×10^{-3}	HEA/Al_2O_3: delamination wear HEA/steel: mild oxidative wear	[60]
$Al_{0.25}Ti_{0.75}CoCrFeNi$	*Arc-melting and casting *Polishing with 0.1 μm silica	/	χ-phase: 1090 HV Heusler: 570 HV	/	*Stroke length: 1 mm *Sliding frequency: 5 Hz *Load: 20 N *Sliding time: 20 min *Sliding distance: 15 m	Specific wear rate: 10 N: 1.2×10^{-5} 15 N: 1.4×10^{-5} 20 N: 1.2×10^{-5}	Mixed mechanisms: 3-body abrasion + surface fatigue + oxidative wear	[29]
$AlCoCrFeNiSi_x$ ($x = 0, 0.5, 1.0, 1.5, 2.0$)	*Arc melting	Effect of silicon	$x = 0$: 500 HV $x = 2$: 908 HV	$x = 0$: 0.58 $x = 2.0$: 0.3	*Velocity: 0.002 m/s *Load: 200 g (1.96 N) *Sliding time: 30 min	In this paper only the mass loss was identified (mg): $x = 0$: 17.9 mg $x = 2.0$: 9.6 mg	Abrasive wear	[30]
$Al_{0.6}CoCrFeNi$	*Arc-melting *Grinding using 360–2500 grit → polishing using 0.2 μm diamond suspension.	Effect of environment and sliding velocity	280 HV	*2 Hz: Air: 0.542, water: 0.203, rain: 0.173, seawater: 0.322 *3 Hz: Air: 0.536, water: 0.196, rain: 0.184, seawater: 0.270 *4 Hz: Air: 0.365, water: 0.149, rain: 0.294, seawater: 0.152 *5 Hz: Air: 0.402, water: 0.200, rain: 0.160, seawater: 0.160	*Sliding velocity: 2, 3, 4, 5 Hz *Sliding time: 1800 s *Reciprocating amplitude: 5 mm *Temperature: 25 °C	*2 Hz x10^{-4}: Air: 6.52, water: 0.198, rain: 0.276, seawater: 0.265 *3 Hz x10^{-4}: Air: 6.36, water: 0.174, rain: 0.128, seawater: 0.165 *4 Hz x10^{-4}: Air: 1.59, water: 148, rain: 0.144, seawater: 0.118 *5 Hz x10^{-4}: Air: 1.90, water: 0.244, rain: 0.220, seawater: 0.201	*Ambient air condition and deionized water: abrasive, delamination, oxidative wear. *Acid rain: corrosion wear, adhesive, abrasive, and oxidative wear.	[56]
$Al_{0.6}CoCrFeNi$	* Arc-melting * Cold rolling at room temperature → annealing at 850 °C for 4 h	Effect of temperature	*As cast $Al_{0.6}CoCrFeNi$:270 *Annealed $Al_{0.6}CoCrFeNi$: 480	Annealed $Al_{0.6}CoCrFeNi$: *At room Temperature: 0.79 *At 800 °C: 0.5	/	Annealed $Al_{0.6}CoCrFeNi$: *At room Temperature: 0.3 × 10-4 *At 800 °C: 5.2 × 10-4	*As the temperature increases, the wear mechanism goes from abrasive to mild oxidative wear	[43]
$Al_{0.25}CoCrFeNi$	*Arc-melting *Thickness reduction of 40% by cold rolling to reduce casting defects →	Effect of temperature	*As cast: 151 HV *After rolling: 365 HV *After rolling + annealing: 260 HV	20 °C: 0.725 100 °C: 0.65 200 °C: 0.62 400 °C: 0.56	Dry sliding wear: *sliding velocity: 0.084 m/s (200 r/min)	20 °C: 1.5×10^{-4} 100 °C: 2.3×10^{-4} 200 °C: 2.75×10^{-4} 400 °C: 3.6×10^{-4}	20 °C: Abrasive wear 200 °C: Delamination 300 °C: Delamination + Oxidative wear	[44]

(*continued on next page*)

Table 2 (*continued*)

Alloy composition	Alloy Preparation	Influencing parameter	Hardness (HV)	Coefficient of friction	Wear test conditions	Specific wear rate ($mm^3/N/m$) or Wear rate (mm^3/m) or Erosion rate (mm^3/h) or Wear resistance (m/mm^3)	Wear mechanism	Ref.
	annealing at 700 °C for 30 min to eliminate residual stresses			500 °C: 0.52 600 °C: 0.51	*Sliding time: 30 min *Load: 10 N	500 °C: 3.4×10^{-4} 600 °C: 3.5×10^{-4}	400, 500, 600 °C: Oxidative wear	
$Al_{0.4}FeCrNiCo_x$ ($x = 0, 0.25, 0.5, 1.0$)	*Arc melting *Grinding (220, 400, 600, 800, 1000 grit) → ultrasonic cleaning in an acetone bath	Effect of cobalt, sliding velocity, load, and sliding distance	$x = 0$: 377.7 HV $x = 1$: 199.5 HV	For 1 m/s, 10 N, 1 Km: $x = 0$: 0.06 $x = 0.25$: 0.07 $x = 0.5$: 0.1 $x = 1$: 0.13	*Sliding velocity: 0.5, 1, 1.5, 2 m/s *Load: 5, 10, 15, 20 N *Distance: 1, 2, 3, 4 Km *Medium: Oil	For 1 m/s, 10 N, 1 Km: $x = 0$: 4.9×10^{-5} $x = 0.25$: 5.5×10^{-5} $x = 0.5$: 6.2×10^{-5} $x = 1$: 7.3×10^{-5}	Adhesive and abrasive wear	[52]
$CoCrFeNiCu_x$ ($x = 0, 0.2, 0.4, 0.6, 0.8, 1.0$)	*Arc melting *Polishing → etching in aqua regia ($HCl:HNO_3$ = 3:1) for 15 *s*	Effect of copper and temperature	$x = 0$: 136 HV $x = 1$: 169 HV	/	*Sliding velocity: 95 rpm *Load: 100 N *Sliding time: 1000s * Temperatures: 25,600 °C	*At 25 °C: $x = 0$: 2.3×10^{-5} $x = 1$: 1.75×10^{-5} *At 600 °C: $x = 0$: 2.4×10^{-5} $x = 1$: 1.3×10^{-5}	From abrasive to adhesive wear with addition of Cu at elevated temperature	[49]
Al_xCoCrFeNi CoCrFeMnNi ($x = 0.3, 0.6, 1.0$)	Vacuum arc-melting *Grinding with 4000 grit → ultrasonic cleaning in ethanol	Effect of aluminium and temperature	CoCrFeMnNi: 225 HV $x = 0.3$: 176 HV $x = 0.6$: 251 HV $x = 1$: 630 HV	For all HEAs: At 600 °C: 0.51 At 800 °C: 0.42 At 900 °C: 0.34	*Velocity: 0.1 m/s *Load: 15 N *sliding distance: 1 km *sliding radius of 5 mm	At all temperatures, ($x = 1$) has exceptional wear resistance compared to all HEAs	Abrasive wear at room temperature → oxidative and delamination wear at high temperature	[50]
$Al_{0.4}FeCrNiCo_x$ ($x = 0, 0.25, 0.5, 1.0$)	*Arc melting *Homogenization at 1100 °C for 24 h in an Ar atmosphere → furnace-cooling. *Polishing (grit size 220, 400, 600, 800, and 1000)–> ultrasonic cleaning in an acetone bath–> drying for 30 min in the furnace at 60 °C	Effect of cobalt, sliding velocity, and load	$x = 0$: 377.7 HV $x = 1$: 199.5 HV	At 5 N: $x = 0$: 0.271 $x = 0.25$: 0.293 $x = 0.5$: 0.296 $x = 1.0$: 0.301 At 20 N: $x = 0$: 0.219 $x = 0.25$: 0.226 $x = 0.5$: 0.232 $x = 1.0$: 0.251	*Velocity: 0.5, 1, 1.5, 2 m/s *Normal load: 5 N, 20 N *Sliding distance: 1 km *Medium: Dry *Temperature: Room T	*0.5 m/s $x = 0$: 2.391×10^{-4} $x = 1$: 3.375×10^{-4} *2 m/s $x = 0$: 4.983×10^{-4} $x = 1$: 7.702×10^{-4} *5 N $x = 0$: 0.704×10^{-4} $x = 1$: 1.175×10^{-4} *20 N $x = 0$: increase with 274.33% $x = 1$: increase with 281.19%	Adhesive wear, plastic deformation, along with delamination. The oxidative wear was also present but less effective in case of lower oxygen and higher cobalt	[53]
$AlCoCrFeNiTi_{0.5}$	*Arc melting → remelting → Annealing at 800 °C for 5 h	Effect of heat treatment (remelting, annealing)	As cast: 650 HV Remelted: 705 HV Annealed: 810 HV	As cast: 0.59 Remelted: 0.53 Annealed: 0.52	*Rotation speed: 200r/min *Load: 100 N *Sliding time: 60 min *Room temperature	Wear mass loss was identified instead of wear rate As cast: 0.4 mg/mm^2 Remelted: 0.25 mg/mm^2 Annealed: 0.15 mg/mm^2	/	[42]

(*continued on next page*)

Table 2 (*continued*)

Alloy composition	Alloy Preparation	Influencing parameter	Hardness (HV)	Coefficient of friction	Wear test conditions	Specific wear rate ($mm^3/N/m$) or Wear rate (mm^3/m) or Erosion rate (mm^3/h) or Wear resistance (m/mm^3)	Wear mechanism	Ref.
$FeCoCrNiMnAl_x$ ($x = 0, 0.5, 1.0$)	*Synthesis in a planetary ball mill for 45 h *Sintering in a vacuum hot-pressing furnace at 900 °C, 1 h under 50 MPa → cooling down to room temperature in the furnace	Effect of aluminium and temperature	*At room Temperature: $x = 1$: 690 HV, $x = 0.5$: 550 HV, $x = 0$: 420 HV *At 500 °C: $x = 1$: 555 HV, $x = 0.5$: 420 HV, $x = 0$: 360 HV *At 800 °C: $x = 1$: 125 HV, $x = 0.5$: 100 HV, $x = 0$: 75 HV	*At room temperature: $x = 1$: 0.31, x = 0.5: 0.32, $x = 0$: 0.25 *At 200 °C: $x = 1$: 0.4, $x = 0.5$: 0.32, $x = 0$: 0.23 *At 500 °C: $x = 1$: 0.28, $x = 0.5$: 0.28, $x = 0$: 0.23 *At 800 °C: $x = 1$: 0.19, $x = 0.5$: 0.19, $x = 0$: 0.26	*Sliding velocity: 0.24 m/s (450 rpm) *Friction radius: 5 mm *Load: 10 N *Sliding time: 15 min	*At room Temperature: ($x10^{-4}$) $x = 1$: 1.00, $x = 0.5$: 1.55, $x = 0$: 2.77 *At 200°C: $x = 1$: 1.25, $x = 0.5$: 2.00, $x = 0$: 3.77 *At 800 °C: $x = 1$: 0.1, $x = 0.5$: 0.25, $x = 0$: 0.25	$x = 0$: Abrasive wear + mild oxidation wear $x = 0.5$: Mild oxidation wear $x = 1.0$: Mild oxidation wear	[51]
$CoCrFeNiMo_{0.2}$	*Spark plasma sintering (SPS) → cold rolling *Polishing (surface roughness less than 100 nm)	*Effect of duration (number of sliding) *Effect of load *Effect of velocity	457.2 HV	*Effect of duration: at 60 cycles: 0.6, at 3600 cycles: 0.625 *Effect of load: under 5 N: 0.719, under 80 N: 0.589 *Effect of velocity: 6 mm/s: 0.611, 240 mm/s: 0.407	*Sliding velocity: 6–240 mm/s *Load: 5–80 N *Sliding time: 60–3600 cycles	*Effect of duration: at 60 cycles: 0.95×10^{-3} 3600: 0.15×10^{-3} *Effect of load: under 5 N: 0.52×10^{-3}, 80 N: 0.3×10^{-3} *Effect of velocity: 6 mm/s: 0.42×10^{-3}, 240: 1.25×10^{-3}	At initial stage of sliding/ under low load: Abrasion wear and plastic deformation. At the dynamic friction equilibrium conditions: oxidation, wand delamination.	[55]
$Al_xCoCrFeNiSi$ ($x = 0, 0.5, 1.0, 1.5, 2.0$)	*Vacuum arc melting	Effect of aluminium	$x = 0.5$: 598 HV $x = 2.0$: 909 HV	$x = 0.5$: 0.45 $x = 2.0$: 0.21	/	In this paper only the mass loss was identified (mg): $x = 0$: 0.035 mg $x = 2.0$: 0.018 mg	Abrasive wear	[32]
TaTiVWZr HfTaTiVZr	*Vacuum arc melting *Annealing at 450 °C for 2 h to investigate the microstructural stability	Effect of temperature	At all temperatures: TaTiVWZr: 826 HV HfTaTiVZr: 694 HV	Slight increase up to 150 °C then slight decrease up to 450 °C *TaTiVWZr:0.25 *HfTaTiVZr: 0.32	*Sliding frequency: 5 Hz *Sliding time: 90 min *Sliding distance: 190 m *Sliding temperatures: 25, 150, 300,450 °C	*At 25 °C: TaTiVWZr: 2.8×10^{-4} HfTaTiVZr: 3.2×10^{-4} At 150 °C: TaTiVWZr: 7.8×10^{-4} HfTaTiVZr: 7.2×10^{-4} *At 450 °C: TaTiVWZr: 1×10^{-4} HfTaTiVZr: 2.3×10^{-4}	From adhesive and abrasive wear to severe oxidative wear	[48]
$CoCrFeMnNiC_x$ ($x = 0, 0.3, 0.6, 0.9, 1.2$)	*Mechanical alloying of (graphene + gas-atomized CoCrFeMnNi) and spark plasma sintering → Polishing	Effect of carbon	$x = 0$: 327.8 HV $x = 0.6$: 566.4 HV	/	*Frequency: 4 Hz *Load: 20 N *Sliding distance: 100 m *Room temperature	$x = 0$: 6.5×10^{-5} $x = 0.6$: 0.47×10^{-5}	From delamination wear to abrasive wear	[41]

(*continued on next page*)

Table 2 (*continued*)

Alloy composition	Alloy Preparation	Influencing parameter	Hardness (HV)	Coefficient of friction	Wear test conditions	Specific wear rate ($mm^3/N/m$) or Wear rate (mm^3/m) or Erosion rate (mm^3/h) or Wear resistance (m/mm^3)	Wear mechanism	Ref.
$Al_{1.8}CrCuFeNi_2$	*Arc melting * Heating with a high-frequency furnace, melting to 1320 °C, 1360 °C, and 1400 °C → water-cooled	Effect of temperature	/	As-cast: 0.29 1320 °C: 0.3 1360 °C: 0.34 1400 °C: 0.36	*Friction time: 60 min *Friction speed: 200 rpm *Load: 100 N * Room temperature * Medium: dry	In this paper only the mass loss was identified (mg): As-cast:5.2 1320 °C: 3.7 1360 °C: 3.5 1400 °C: 3.2	The adhesive wear mechanism for $Al_{1.8}CrCuFeNi_2$ is mainly delamination wear	[45]
$CrFeNiAl_{0.4}Ti_{0.2}$	*Arc melting → Re-melting, casting and flipping over at least 6 times → homogenization at 1100 °C in a tube furnace for 6 h in Argon	Effect of temperature	As cast HEA: 552 HV Homogenized HEA: 525 HV	600 °C: 0.41 700 °C: 0.45 800 °C: 0.5 900 °C: 0.43 950 °C: 0.417	Reciprocating dry sliding: *Normal load: 20 N *Frequency: 1 Hz *Sliding time: 20 min *Stroke length: 7 mm	600 °C: 22.5×10^{-5} 700 °C: 15×10^{-5} 800 °C: 1.61×10^{-5} 900 °C: 16×10^{-5} 950 °C: 45×10^{-5}	*At 600 °C abrasion wear *At high temperature, 800–950 °C: oxidation wear	[46]

phase) and ordered BCC (B2 phase) for $Al_{0.7}CoCrFeNi$. The increase of Al causes chemical segregations, and thus localized corrosion in the form of pitting which propagates in the chromium depleted BCC phase in $Al_{0.5}CoCrFeNi$ and $Al_{0.7}CoCrFeNi$ [65]. For that reason, heat treatment at 1250 °C seems to be an effective way to enhance the corrosion resistance of the $Al_xCoCrFeNi$ HEAs in 3.5 wt% NaCl solution by generating a homogenization effect [64].

Wang et al. [66] investigated the corrosion resistance of the AlCoCrFeNi HEA in 0.6 M sodium chloride solution after aging at different temperatures (800, 1000 and 1200 °C) for 168 h. The electrochemical parameters of the alloy aged at 800 °C are comparable to the ones of the sample aged at 1000 °C. The alloy aged at 1200 °C exhibits higher corrosion potential and lower corrosion current density. At the three studied aging temperatures, AlCoCrFeNi experiences galvanic corrosion due to the formation of a galvanic potential between the (Al-Ni)-rich matrix and the (Fe-Cr)-rich precipitates. Compared to the 304 stainless steel, the corrosion resistance of the three AlCoCrFeNi specimens is lower than that of the commercial alloy.

The dependence of the microstructural features e.g., lattice type and grain size, on the corrosion behaviour of the sequentially alloyed AlCoCrFeNi HEA was investigated [67]. Polarization measurements were performed in 3.5 wt% sodium chloride solution at room temperature. The sequence of producing AlCoCrFeNi HEA affected the resulting phases ratio of the alloy. In fact, the sequence CoNi→Fe→Cr→Al produced CoNiFeCrAl with 84% of BCC and 16% of FCC; FeCr→Ni→Al→Co produced FeCrNiAlCo consisting of 62% of BCC; and AlNi→Co→Cr→Fe resulted in 38% of BCC structure. Depending on the lattice, two competing factors play a significant role in the corrosion behaviour: (1) FCC is better for corrosion resistance than BCC due to the compactness of FCC; (2) FCC is enriched in iron, chromium and nickel which can readily decrease the corrosion resistance due to the segregation phenomenon. The overlap of these factors is responsible for the lower corrosion current density and the higher corrosion potential of FeCrNiAlCo compared to CoNiFeCrAl and AlNiCoCrFe. In addition, the larger the grain size, the higher the corrosion resistance is. In fact, the three sequential alloys exhibit comparable BCC grain sizes; however, the FCC grain size in CoNiFeCrAl and FeCrNiAlCo is higher than that in AlNiCoCrFe. Therefore, excellent corrosion resistant HEAs can be prepared by controlling the BCC:FCC ratio via heat treatment in order to obtain larger grain sizes.

The microstructure of the $AlCrFeCoNiSi_{0.1}$ HEA is composed of dendritic and interdendritic phases, both having an (AlNi)-rich matrix with ordered BCC (B2) lattice, and (FeCr)-rich precipitates with disordered BCC (A2) lattice [68]. The pits growth takes place in the Cr-deficient dendritic regions, and a galvanic potential occurs between the dendritic and the interdendritic phases resulting in galvanic corrosion in the interdendrites. The potentiodynamic test in chloride media indicates that the corrosion potential of $AlCoCrFeNiSi_{0.1}$ is slightly higher than that of the 304 stainless steel, and the corrosion current density is about three times higher than that of the commercial alloy. The AlCrFeCoNiCu HEA, another derivative of AlCrFeCoNi, was synthetized, remelted, and then annealed, and the corrosion resistance was assessed in each step in a 3.5% NaCl solution [69]. It was found that the annealed HEA has the best corrosion resistance because the dendrite phase grows larger after annealing than after remelting.

Chen et al. [70] investigated the electrochemical properties of $AlCrFeCoNiCu_{0.5}Si$. The test solution was either composed of pure H_2SO_4, pure NaCl or the mixture of 1 N H_2SO_4 with different concentrations of NaCl (0.01, 0.1, 0.4, 0.5, 0.6, 1.0 M). The results showed that the HEA has higher resistance to general corrosion than the 304 stainless steel in chloride and sulfuric media at all concentrations. However, $AlCrFeCoNiCu_{0.5}Si$ is more prone to pitting corrosion due to the low pitting potential in chloride medium. When 1 N H_2SO_4 was mixed with 1 M NaCl the corrosion rate decreased by 44% compared to 1 N H_2SO_4 chloride-free, but it was still higher than that in 1 M NaCl. Furthermore, when mixing 1 N H_2SO_4 with 0.5 M NaCl, solution similar to seawater, the HEA had lower resistance to general corrosion. Compared to 1 M NaCl sulphate-free, when adding 1 N H_2SO_4 to 1 M NaCl the corrosion potential increased and moved to nobler values due to the inhibitory character of SO_4^{2-} ions which tend to block pitting corrosion caused by Cl^- ions.

It has been seldom considered that the addition of Al improves the pitting resistance of HEAs. $Al_xCrFeMoV$ HEAs ($x = 0$, 0.2, 0.6, 1.0 in molar ratio) show high corrosion resistance, especially to pitting corrosion, when increasing the aluminium content [71]. This is attributed to their high pitting resistant equivalent number (PREN) and the absence of any Al-rich phase. The equiatomic molybdenum and chromium contents are responsible for the decrease of pitting corrosion since Mo^{4+} and Cr^{3+} provide better passivation resistance and withstand the pit growth.

There are only few papers published investigating the corrosion performance of the $Al_xCoCrFeNiTi_{0.5}$ ($x = 0$, 0.5, 1.0 in molar ratio) HEAs. Zhang et al. [72] are the first authors who studied the influence of adding aluminium and titanium on the CrFeCoNi system to investigate the corrosion behaviour of $Al_xCoCrFeNiTi_{0.5}$ ($x = 0$, 0.5, 1.0 in molar ratio) in 0.5 M H_2SO_4. The aluminium-free $Al_xCoCrFeNiTi_{0.5}$ HEA showed higher pitting corrosion than $Al_{0.5}CoCrFeNiTi_{0.5}$ and $AlCoCrFeNiTi_{0.5}$, indicating that a higher content of aluminium enhanced the corrosion resistance of the HEA. Furthermore, $Al_{0.5}CoCrFeNiTi_{0.5}$ and $AlCoCrFeNiTi_{0.5}$ HEAs had better corrosion resistance at room temperature than the 304 stainless steel.

Qiu et al. [73] investigated the effect of Al and Ti on the microstructure and on the electrochemical and corrosion properties of $Al_xCoCrFeNiTi_y$ ($x = 0.3$, 0.6, 0.9 and $y = 0$, 0.5 in molar ratio). Four HEAs were prepared: $Al_{0.3}CoCrFeNi$, $Al_{0.6}CoCrFeNi$, $Al_{0.9}CoCrFeNi$ and $Al_{0.9}CoCrFeNiTi_{0.5}$. Both $Al_{0.6}CoCrFeNi$ and $Al_{0.9}CoCrFeNi$ exhibited higher corrosion potential and lower corrosion current densities than the $Al_{0.3}CoCrFeNi$ HEA. This fact is due to the complex microstructure of the former alloys, having BCC, FCC and B2 phases; while $Al_{0.3}CoCrFeNi$ consists just of a single disordered FCC phase. The high corrosion current density makes $Al_{0.9}CoCrFeNiTi_{0.5}$ more prone to general corrosion in 0.6 M NaCl solution compared to the other compositions. This may be ascribed to the formation of a chromium depleted zone due to the presence of intermetallic phases such as iron-chromium phase (σ-phase).

Wang et al. [74] monitored the evolution of the microstructure and corrosion behaviour of the $Al_{0.6}CoFeNiCr_{0.4}$ HEA. It was produced by arc melting and then subjected to heat treatments in the range of 550–850 °C for 24 h. Depending on the aging temperature, five HEAs were generated: the as-cast alloy, and the alloys aged at 550, 650, 750, and 850 °C. During aging the crystal structure of the $Al_{0.6}CoFeNiCr_{0.4}$ HEA first transformed from FCC(Fe-Cr) + disordered BCC phase to FCC + disordered BCC + ordered B2 (Al-Ni), and then to FCC + ordered B2 structure. According to the corrosion potential and corrosion current density values at

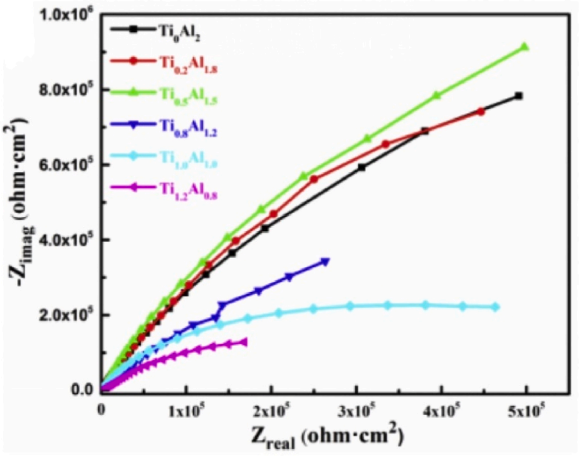

Fig. 8. Nyquist plot of $Al_{2-x}CoCrFeNiTi_x$ as-cast HEAs. Reproduced with permission from Ref. [75].

different aging temperatures in 3.5 wt% NaCl solution, $Al_{0.6}CoFeNiCr_{0.4}$ aged at 550 °C showed the best corrosion resistance. In fact, the corrosion resistance could be ordered according to the following graduation: aged at 550 °C > aged at 650 °C > as-cast > aged at 750 °C > aged at 850 °C. This could be related to the presence of the ordered B2 phase richer in Al, which indicates that the phase containing much more Al is susceptible to corrosion in the presence of chloride ions.

By modifying simultaneously the Al and Ti content in the $Al_{2-x}CrFeCoNiTi_x$ ($x = 0$, 0.2, 0.5, 0.8, 1.0, 1.2 in molar ratio) HEAs, it was observed that the passivation resistance increased when the titanium-to-aluminium molar ratio increased from $x = 0$ to $x = 0.5$, as inferred from the Nyquist plot shown in Fig. 8 [75]. The radius of the impedance arc in the Nyquist plot is an indicator of the polarization resistance and the status of the oxide layers formed on the surface. The radius of the impedance arc starts to be smaller between $x = 0.8$ and $x = 1.2$, meaning that the $Al_{1.5}CrFeCoNiTi_{0.5}$ HEA exhibits the best passivation resistance among all the evaluated HEAs. This occurs despite the fact that its microstructure consists of Fe-Cr, Al-Ni and Laves phases, which may have a detrimental effect on the stability of the passive layer. The results of the potentiodynamic tests performed in 3.5 wt% sodium chloride solution indicate that the addition of Ti makes $Al_{2-x}CrFeCoNiTi_x$ resistant to pitting corrosion.

The corrosion resistance of CuYZrTiHf, CuYZrAlHf, and CuYZrAlTi was investigated in artificial seawater solution (3.5 wt% of salt ions) at room temperature [76]. The artificial sea salt consists of NaCl, $MgCl_2$, $MgSO_4$ and $CaCl_2$. The Ti-Hf-containing HEA and Al-Hf-containing HEA exhibit higher corrosion potentials and lower corrosion current densities than the CuYZrAlTi HEA. However, this latter has the highest resistance to pitting corrosion since it shows higher pitting potential and wider passive region.

3.1.2. Effect of Ti content

The corrosion behaviour of $AlCrFeCoNiTi_x$ ($x = 0$, 0.4, 0.8. 1.0 in molar ratio) in 3.5 wt% sodium chloride solution was investigated [77]. The quantity of pits formed on the surface of $AlCrFeCoNiTi_x$ increased as the amount of Ti increased. For AlCrFeCoNi, the corroded surface showed numerous small pits, while $AlCrFeCoNiTi_{0.8}$ and AlCrFeCoNiTi exhibited significant pits which resulted in more damage on the surface. It is presumed that the stability of the titanium-based intermetallic compounds formed in $AlCrFeCoNiTi_x$ HEAs had a direct consequence in increasing the corrosion resistance. However, $AlCrFeCoNiTi_{0.4}$ did not show any evident corrosion pits. Therefore, the optimum composition with the best corrosion performance was $AlCrFeCoNiTi_{0.4}$.

The corrosion behaviour of $AlCrFeCoNiMo_{0.5}Ti_x$ ($x = 0$, 0.25, 0.3, 0.4, 0.5 in molar ratio) in 3.5 wt% NaCl solution was also investigated [78]. The corresponding impedance arc become larger as the amount of Ti increased, and thus the passivation resistance of $AlCrFeCoNiMo_{0.5}Ti_x$ become substantially higher. Furthermore, both the pitting potential and corrosion potential increased, and the corrosion current density decreased indicating that the corrosion resistance of the $AlCrFeCoNiMo_{0.5}Ti_x$ HEAs was improved by increasing the Ti content. Kukshal et al. [79] reported that the addition of Ti can also enhance the corrosion behaviour of $AlCr_{1.5}CuFeNi_2Ti_x$ ($x = 0$, 0.25, 0.5, 0.75, 1.0 in molar ratio) when the HEAs are immersed in 3.5 wt% NaCl solution at room temperature. However, Xiao et al. [80] reported that the addition of Ti decreases the corrosion resistance of the AlCoCuFeNiTi HEA in 0.5 M H_2SO_4 solution at 25 °C.

3.1.3. Effect of Mo

The corrosion resistance of the $CoCrFeNi_2Mo_x$ ($x = 0$, 0.25 molar ratio) HEAs was investigated in simulated seawater, and their performance was compared to the nickel-molybdenum-chromium HASTELLOY® superalloy and iron-chromium-nickel 316L stainless steel [81]. $CoCrFeNi_2$ and 316L exhibit unstable passivation layer on the surface under the harsh attack of NaCl. That fact results in the formation of pits measuring 0.19 μm and 0.03 μm in size, respectively. On the other hand, $CrFeCoNi_2Mo_{0.25}$ and HASTELLOY® have no cracks or pits on their surfaces. The addition of 0.25 mol of Mo improves the stability of the Cr_2O_3-based oxide layer and increases the breakdown potential by precipitating MoO_2 oxides.

Another similar study was done by investigating the corrosion behaviour of $CrFeCoNiMo_x$ ($x = 0.1$, 0.2, 0.3, 0.4, 0.5) [82]. When

increasing the Mo content, the precipitated (Cr, Mo) rich σ-phase increases. This phase is responsible for the improvement in wear resistance due to its high hardness and also fosters the formation of galvanic corrosion in 3.5 wt% NaCl and 0.5 mol/L H_2SO_4. However, the addition of Mo decreases the corrosion current density and increases the corrosion potential. Among the five studied HEAs $CoCrFeNiMo_{0.2}$ and $CoCrFeNiMo_{0.4}$ depicted the best corrosion resistance. This is believed to be related to the optimal proportion of σ-phase and the Mo content. Potentiodynamic tests in 0.25 M and 1 M NaCl solutions were carried out to investigate the effect of Mo on the corrosion behaviour of $CrFeCoNiMo_x$ (x = 0, 0.1, 0.3, 0.6 molar ratio) [2]. The addition of Mo decreased the corrosion current density and improved the stability of the passive layer of the molybdenum-free $CrFeCoNiMo_x$ in a higher degree than of the alloy $CrFeCoNiMo_{0.1}$; however, both showed pitting corrosion. In $CrFeCoNiMo_{0.3}$ and $CrFeCoNiMo_{0.6}$ the electrochemical alteration occurred when the regions around the Cr-Mo enriched precipitates were depleted of these two elements. The $CrFeCoNiMo_x$ (x = 0, 0.2, 0.5, 0.8, 1.0 molar ratio) HEAs were prepared by arc melting followed by homogenization annealing [83]. The corrosion behaviour of the as-annealed alloys was investigated in seawater solution. With the addition of Mo, the corrosion potential E_{corr} increased from −1.048 V for the Mo-free HEA to −1.034 V for $CrFeCoNiMo_{0.5}$ and decreased to −1.077 V for CrFeCoNiMo. The$CrFeCoNiMo_{0.5}$ HEA had the lowest corrosion current density suggesting that $CrFeCoNiMo_{0.5}$ exhibited the best uniform corrosion in seawater solution among the tested HEAs.

A new eutectic $Fe_2Ni_2CrMo_x$ (x = 0.25, 0.50, 0.75, 1.0, 1.25, 1.5) HEA family was recently developed [84]. Only the microstructure and the mechanical properties were investigated, therefore corrosion resistance investigations are still needed. In that regard, Godlewska et al. [85] found that minor quantities of Mo improve the corrosion resistance by hindering the pit growth of $AlCrFe_2Ni_2Mo_x$ (x = 0, 0.05, 0.1, 0.15 molar ratio), in simulated chloride environment at ambient temperature.

Chou et al. [86] reported that the Mo-free $Co_{1.5}CrFeNi_{1.5}Ti_{0.5}Mo_x$ (x = 0, 0.1, 0.5, 0.8 molar ratio) HEA withstands general corrosion better than the $Co_{1.5}CrFeNi_{1.5}Ti_{0.5}Mo_{0.1}$, $Co_{1.5}CrFeNi_{1.5}Ti_{0.5}Mo_{0.5}$, and $Co_{1.5}CrFeNi_{1.5}Ti_{0.5}Mo_{0.8}$ HEAs in simulated basic (NaOH) and acidic (H_2SO_4) media at room temperature. However, according to the cyclic polarization curves, the positive hysteresis for $Co_{1.5}CrFeNi_{1.5}Ti_{0.5}$, and the negative hysteresis for $Co_{1.5}CrFeNi_{1.5}Ti_{0.5}Mo_x$ (x = 0.1, 0.5, 0.8 molar ratio) prove that the addition of Mo improves the pitting corrosion in simulated marine environment (1 M NaCl). The pitting potential E_{pit} is determined when the current density begins to increase considerably in the passive range because of the formation of pits on the passive layer. The potential difference ΔE_{pit} between the pitting potential E_{pit} and the corrosion potential E_{corr} represents the stability and resistance to passive layer breakdown. Larger ΔE_{pit} values indicate higher resistance to pit growth, which in turn is related to the stability of the passive film. ΔE_{pit} of the $Co_{1.5}CrFeNi_{1.5}Ti_{0.5}Mo_{0.1}$ HEA declines when the concentration of Cl^- ions increases and the temperature increases from room temperature to 80 °C [87].

3.1.4. *Effect of Cu*

Regarding the influence of copper addition on the corrosion resistance of the $CrFeCoNiCu_x$ (x = 0, 0.5, 1.0 molar ratio) HEAs, it was found that an increase in Cu content leads to an increase in the quantity of Cu precipitates at the grain boundaries [88]. The interdendritic phase becomes enriched in Cu and the dendritic phase becomes a Cu-depleted region, which is in accordance with the study performed by Verma et al. [49]. The increment of segregation of Cu in the interdendritic phase of $CrFeCoNiCu_x$ impedes the formation of a protective passive layer against corrosion deterioration. This explains the fact that the Cu-free $CrFeCoNiCu_x$ HEA has the tendency to passivate more easily than the Cu-containing HEAs in chloride media. When the amount of Cu increases, the corrosion resistance decreases substantially [88]. Based on the results of immersion tests in 3.5 wt% sodium chloride solution, the predominant type of corrosion detected in CrFeCoNiCu is localized corrosion. Fig. 9 depicts a schematic illustration of the process occurring during the corrosion of CoCrFeNiCu in 0.6 M NaCl. Before corrosion starts (Fig. 9a), two oxide layers are formed on the HEA: Cr_2O_3, which is known for its resistance to Cl^- ions; and Cu_2O, which easily dissolves in chloride media. During corrosion (Fig. 9b), the oxidation of copper takes place in the areas enriched in Cu, and a galvanic cell occurs between the Cu-rich (acting as the anode) and the Cu-depleted region. After corrosion (Fig. 9c), Cr_2O_3 oxide film is formed, especially in the zones enriched in chromium. To improve the corrosion

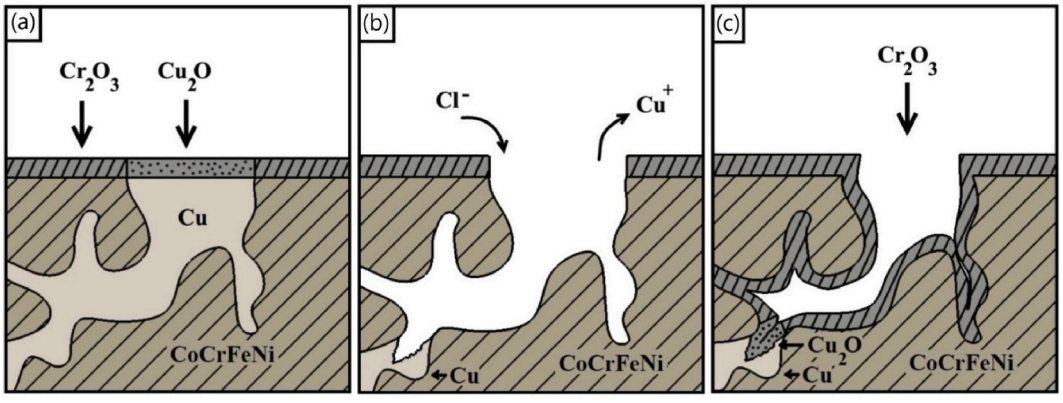

Fig. 9. A schematic illustration of the proposed process occurring during the corrosion of CoCrFeNiCu in 0.6 M NaCl, a) before corrosion; b) during corrosion; c) after corrosion. Reproduced with permission from Ref. [3].

resistance of the Cu-containing HEAs, Cr can be added since it improves the chemical properties of the oxide layers formed on the surfaces of the alloys [3].

Comparing the corrosion behaviours of FeNiCoCrCu and FeNiCoCrMn, it was found that FeNiCoCrCu tends to withstand corrosion in extremely aggressive solutions, like 5% and 10% HCl, HNO_3, and H_2SO_4 solutions. FeNiCoCrCu exhibits lower weight loss rates after 24–120 h of exposure and thus, lower corrosion rates [89].

3.1.5. Effect of C

Luo et al. [90] investigated the effect of adding carbon on the corrosion resistance of the CrFeCoNiMn system. As the amount of C in the interstitial equiatomic $CoCrFeMnNiC_x$ ($x = 0$, 0.2, 0.5, and 0.8 atomic ratio) HEAs increases from 0 to 0.5 at.%, the resistance to pitting corrosion increases. Then the corrosion resistance decreases when the content of C reaches 0.8 at.%. The open circuit potential (OCP) measurements in 3.5 wt% NaCl-saturated $Ca(OH)_2$ solution show that the addition of 0.2 at.% and 0.5 at.% of carbon improves the stability of the passive layer formed on the surface of the alloys. The high-level of passivation is attributed to the presence of Cr, Co and to the high Cr + Ni + Co/Mn + Fe ratio. In fact, Cr, Co and Ni significantly improve corrosion resistance, while Mn and Fe have deleterious effects on the alloy in solution. The Cr/Fe ratio seems to be a strong criterion in investigating the corrosion resistance, since an increase in the Cr/Fe ratio can enhance the pitting potential. For this reason, the Cr + Co + Ni/Fe + Mn ratio is selected to assess the pitting resistance of $CoCrFeMnNiC_x$ ($x = 0.2$, 0.5, and 0.8 atomic ratio), as shown in Fig. 10. The cation fraction ratio increases from 0 to 0.5 at% C and then decreases from 0.5 to 0.8 at% C while the Co content is the lowest when the addition of C is 0.8 at%.

Besides manganese (Mn), Liu et al. [91] added Cu and C to the CrFeCoNi system and investigated the corrosion resistance of the CrFeCoNiMnCuC HEA. After four days of immersion in various acid environments, the weight loss of the alloy was only 3% in 10% nitric acid liquid mixed with 3% of hydrogen fluoride, 0.3% in 10% sulfuric acid liquid, 0.6% in 5% hydrochloric acid liquid and only 0.64% in 10% hydrogen fluoride liquid.

3.1.6. Effect of Nb

By replacing copper with niobium (Nb) in the $CrFeCoNiCu_x$ system, the microstructure changes drastically due to the formation of a new phase having an HCP lattice. Tsau et al. [92] investigated the corrosion behaviour of $CrFeCoNiNb_x$ ($x = 0.2$, 0.4, 0.6, 1.0 molar ratio). The dendritic phase of $CrFeCoNiNb_{0.2}$ and $CrFeCoNiNb_{0.4}$ consists of an FCC structure, and the dendrites of $CrFeCoNiNb_{0.6}$ and CrFeCoNiNb (both Laves phase) consist of an HCP structure. The interdendritic structure of all the HEAs comprises two dominant phases, FCC and HCP (Laves phase). After polarization tests in 1 M sulfuric acid solution at 30 °C and in 1 M sodium chloride solution at 30 °C, the FCC dendrites of $CrFeCoNiNb_{0.2}$ are more deeply attacked by corrosion than the Laves phase in the interdendrite regions. For $CrFeCoNiNb_{0.4}$ the FCC dendrites start to disappear due to the corrosive action of both media. For $CrFeCoNiNb_{0.6}$ and CrFeCoNiNb, no significant change occurred on the Laves phase of the dendritic regions. Although the hardness of the $CrFeCoNiNb_x$ HEAs increases substantially by adding Nb, they showed a slight drop in corrosion resistance. However, the corrosion resistance of $CrFeCoNiNb_x$ is higher than that of the 304 stainless steel. On the other hand, 0.25 M ratio of Nb was added to CrFeCoNiMn system to investigate the oxidation resistance at elevated temperature [93]. The microstructure of $CrFeCoNiMnNb_{0.25}$ consists of a duplex-phase structure of FCC and HCP (Laves phase). The increase of the Nb content and the oxidation temperature promotes the precipitation of Laves phase responsible for the oxidation resistance of $CrFeCoNiMnNb_{0.25}$ at 700 and 800 °C.

When 0.5 mole of niobium and 0.5 mole of molybdenum are added to the FeCoNi system, the $FeCoNiMo_{0.5}Nb_{0.5}$ HEA is obtained, having a dendritic dual phase microstructure responsible for the decreased corrosion resistance of this HEA [94]. However, in 1 M H_2SO_4 and 1 M NaCl solutions, the corrosion potential of $FeCoNiMo_{0.5}Nb_{0.5}$ HEA is nobler than that of the 304 stainless steel, and the corrosion current density exhibits smaller values. This fact suggests that the $FeCoNiMo_{0.5}Nb_{0.5}$ HEA has better corrosion resistance than the commercial alloy. Furthermore, adding Nb/Mo increases the hardness considerably from 112 HV for FeCoNi to 629 HV for

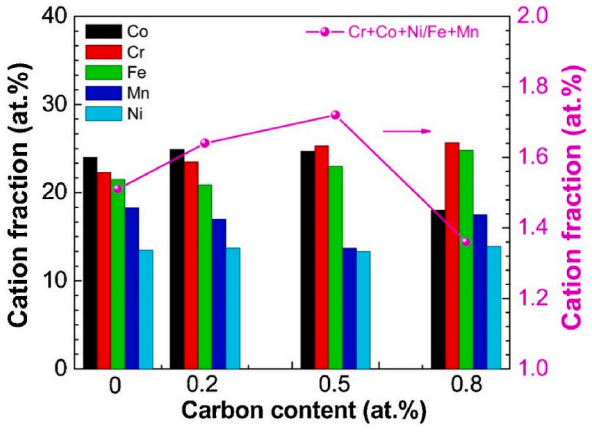

Fig. 10. Cationic fraction ratio in the passive layer of CoCrFeMnNi HEA with various carbon contents after passivation in saturated $Ca(OH)_2$ solution containing 3.5 wt% NaCl. Reproduced with permission from Ref. [90].

$FeCoNiMo_{0.5}Nb_{0.5}$ HEA.

The nanostructured $CrFeCoNiNb_{0.5}$ EHEA consists of Laves phase (Nb-rich) and FCC Nb-depleted phase with a typical lamellar eutectic structure [95]. According to the Nyquist plots and potentiodynamic polarization cyclic curves in 1 M sodium chloride solution, the $CrFeCoNiNb_{0.5}$ EHEA displays high corrosion resistance and excellent self-repair capability compared to the 304 stainless steel. This is due to the combined effect of the nanostructure of the eutectic high entropy alloy and its compact oxide layer. Recently, it has been reported that the corrosion resistance of the $FeCrNiCoNb_{0.5}$ EHEA can be controlled by tuning the size of the eutectic structure (microstructure refinement) in 1 M NaCl [96]. After refinement, potentiodynamic parameters such as transpassivation potential and corrosion current density are improved due to the formation of a thick and compact passive layer which withstands chloride ions adsorption.

Wang et al. [36] investigated the corrosion resistance of the $CrFeCoNiNb_x$ ($x = 0.38$ and 0.54) HEAs. Like $CrFeCoNiNb_{0.5}$, the hypoeutectic $CrFeCoNiNb_{0.38}$ and the hypereutectic $CrFeCoNiNb_{0.54}$ HEAs have lamellar eutectic structure. Moreover, they exhibit excellent corrosion resistance in 3.5 wt% sodium chloride solution. However, the $CrFeCoNiNb_{0.54}$ HEA shows slightly higher corrosion potential compared to $CrFeCoNiNb_{0.38}$.

3.1.7. Effect of other elements

The impedance arc of $Al_{0.5}CoCrCuFeNiB_x$ ($x = 0$, 0.2, 0.6, 1.0 molar ratio) is getting larger as the amount of boron decreases due to the decrease of the passivation resistance of the alloy. Therefore, the corrosion resistance decreases by adding boron, especially when $x \geq 0.6$ mole [97]. Under aqueous acidic conditions, the boron-free $Al_{0.5}CoCrCuFeNi$ HEA exhibits higher corrosion resistance than that of the 304 stainless steel, since it shows high corrosion potential and low current corrosion density compared to the commercial alloy.

By investigating the influence of tin (Sn) in the corrosion resistance of $FeCoNiCuSn_x$ ($x = 0$, 0.02, 0.03, 0.04, 0.05, 0.07, 0.09 molar ratio) in 3.5 wt% sodium chloride solution, it was reported that the addition of small quantities of Sn decreases the corrosion potential. It also increases the corrosion current density, thus decreasing the corrosion resistance [98]. However, $FeCoNiCuSn_{0.04}$ has the best corrosion resistance among all the other compositions; also, the corrosion resistance of $FeCoNiCuSn_x$ in general is higher than that of the 304 stainless steel.

Kukshal et al. [99] investigated the influence of manganese on the corrosion resistance of the $AlCr_{1.5}CuFeNi_2Mn_x$ ($x = 0$, 0.25, 0.5, 0.75, 1.0 molar ratio) HEAs. According to the potentiodynamic tests in 3.5 wt% sodium chloride solution, the addition of Mn at ambient temperature increases the corrosion resistance. This happens because the addition of Mn facilitates the formation of solid solution resulting in the increase of the corrosion resistance. Furthermore, the addition of a high quantity of Mn fosters the optimal distribution of nickel and chromium along the matrix of $AlCr_{1.5}CuFeNi_2Mn_x$, resulting in an enhancement of the electrochemical parameters. The corrosion behaviour of the $AlCrFeCuMnW_x$ ($x = 0$, 0.05, 0.1, 0.5, 1.0 molar ratio) HEA in a 3.5 wt% sodium chloride solution was also investigated [100]. The addition of tungsten improves the corrosion resistance considerably due to the formation of a passive oxide layer of WO_3, which increases as the amount of W increases. Also, W improves the pitting and passivation resistance of $CrFeCoNiW_x$ ($x = 0$, 0.2, 0.5 molar ratio) in seawater environment [101].

The corrosion resistance of AlCoCuFeNi improves when chromium is added to the system [80]. The corrosion rate of the AlCoCuFeNiCr HEA is lower than that of the Cr-free HEA in 0.5 M H_2SO_4 solution at 25 °C because Cr has the tendency to form Cr_2O_3. However, the corrosion rate increases when the temperature reaches 93 °C due to the breakdown of the Cr_2O_3 based passive film. The effect of the chromium content on the corrosion resistance of $AlCr_xFeNi_2Cu_{1.6}$ ($x = 0.5$, 1.5, 2.5 molar ratio) was investigated by Yang et al. [102]. All the studied HEAs had the same microstructure, composed of dendrites with FCC lattice, and an interdendrite phase having BCC lattice. According to the potentiodynamic tests performed in 3.5 wt% sodium chloride solution at room temperature, it was found that the breakdown potential increased and the corrosion current density decreased when the amount of Cr increased. The presence of Cu in $AlCr_xFeNi_2Cu_{1.6}$ may lead to its segregation causing localized corrosion between the matrix and the region where the Cu was segregated. However, copper is distributed evenly along the dendritic region, especially in $AlCr_{2.5}FeNi_2Cu_{1.6}$, due to the high amount of Cr, which hinders this phenomenon of segregation. As a result, the number of pits decreases by adding Cr. According to Yan et al. [103] the change of Cr content in $Al_{0.3}Cr_xFeCoNi$ ($x = 0$, 0.5, 1.0, 1.5, 1.7, 2.0 molar ratio) has a significant effect on the corrosion resistance in chloride media. Also, the HEAs show excellent polarization and passivation resistance, especially when the chromium content is high. The pitting corrosion resistance of all the studied HEAs was enhanced by adding Cr. Moreover, when the chromium content ranged from $x = 1.5$ to $x = 2.0$, a protective oxide layer of Cr_2O_3 was formed leading to an exceptional pitting resistance of the alloy.

The same results were obtained when investigating the influence of the cobalt addition on the corrosion behaviour of $CrFeCo_xNiCuMn$ ($x = 0.5$, 1.0, 1.5, 2.0 molar ratio) [104]. The microstructure of these HEAs consists of two FCC phases; one is enriched in Cr and Fe, the second is enriched in the rest of the elements present in these HEAs (Co, Ni, Cu, and Mn). According to the potentiodynamic polarization measurements carried out in 3.5 wt% sodium chloride solution at room temperature, the electrochemical parameters were improved by the addition of Co. Furthermore, the corrosion resistance was also significantly improved, as inferred from the large radius of the impedance arc in the Nyquist plot and the increase of the passive layer thickness. This fact may be ascribed to the presence of the second FCC phase enriched in Co, Ni, Cu, and Mn.

Microstructure, mechanical properties and corrosion resistance were investigated when combining the effect of Cr, Ti and V on the MoNbFe system [105]. Three HEAs were designed using the Calphad method, namely MoNbFeCrV, MoNbFeCrTi and MoNbFeVTi. The three HEAs have a dominant BCC phase and exhibit a passivation behavior in 1 M sodium chloride and 0.5 M sulfuric acid solutions. It was proven that the designed HEAs showed better corrosion resistance than the 304 stainless steel. However, the potentiodynamic curve of the MoNbFeCrV HEA showed a breakdown potential due to the preferential dissolution of the σ-phase rich in vanadium. Moreover, no signs of pitting corrosion were detected in any of the three alloys.

Table 3
Summary of the most common HEAs used for corrosion resistance.

HEA (x in molar ratio)	Fe	Ni	Cr	Co	Al	Ti	Mo	Mn	Cu	Nb	Si	B	V	W	Sn	C	Ref.
$Cu_{0.5}NiAlCoCrFeSi$	Fe	Ni	Cr	Co	Al				$Cu_{0.5}$		Si						[70]
$FeCoNiCrCu_x$ ($x = 0, 0.5, 1.0$)	Fe	Ni	Cr	Co					**Cu_x**								[88]
$Al_{0.5}CoCrCuFeNiB_x$ ($x = 0, 0.2, 0.6, 1.0$)	Fe	Ni	Cr	Co	$Al_{0.5}$				Cu			**B_x**					[97]
$Al_xCrFe_{1.5}MnNi_{0.5}$ ($x = 0, 0.3, 0.5$)	$Fe_{1.5}$	$Ni_{0.5}$	Cr		**Al_x**			Mn									[61]
$Al_xCrFe_{1.5}MnNi_{0.5}$ ($x = 0, 0.3, 0.5$)	$Fe_{1.5}$	$Ni_{0.5}$	Cr		**Al_x**			Mn									[62]
$Co_{1.5}CrFeNi_{1.5}Ti_{0.5}Mo_x$ ($x = 0, 0.1, 0.5, 0.8$)	Fe	$Ni_{1.5}$	Cr	$Co_{1.5}$		$Ti_{0.5}$	**Mo_x**										[86]
$Co_{1.5}CrFeNi_{1.5}Ti_{0.5}Mo_{0.1}$	Fe	$Ni_{1.5}$	Cr	$Co_{1.5}$		$Ti_{0.5}$	$Mo_{0.1}$										[87]
$NiCoCrFeMnCuC$	Fe	Ni	Cr	Co				Mn	Cu							C	[91]
$AlCrFeCuCo$	Fe		Cr	Co	Al				Cu								[107]
$Al_xCoCrFeNiTi_{0.5}$ ($x = 0, 0.5, 1.0$)	Fe	Ni	Cr	Co	**Al_x**	$Ti_{0.5}$											[72]
$FeCoNiCuSn_x$ ($x = 0, 0.02, 0.03, 0.04, 0.05, 0.07, 0.09$)	Fe	Ni		Co					Cu						**Sn_x**		[98]
$AlCoCrFeNi$	Fe	Ni	Cr	Co	Al												[66]
$AlCoCuFeNiCr$	Fe	Ni	Cr	Co	Al				Cu								[80]
$AlCoCuFeNiTi$	Fe	Ni		Co	Al	Ti			Cu								[80]
$Al_xCoCrFeNi$ ($x = 0.3, 0.5, 0.7$)	Fe	Ni	Cr	Co	**Al_x**												[63]
$Al_{0.1}CoCrFeNi$	Fe	Ni	Cr	Co	$Al_{0.1}$												[108]
$AlCrFeNiMo_{0.5}Ti_x$ ($x = 0, 0.25, 0.3, 0.4, 0.5$)	Fe	Ni	Cr		Al	**Ti_x**	$Mo_{0.5}$										[78]
$FeCoNiNb_{0.5}Mo_{0.5}$	Fe	Ni		Co			$Mo_{0.6}$			$Nb_{0.5}$							[94]
$AlCr_{1.5}CuFeNi_2Ti_x$ ($x = 0, 0.25, 0.5, 0.75, 1.0$)	Fe	Ni_2	$Cr_{1.5}$		Al	**Ti_x**			Cu								[79]
$Al_xCoCrFeNi$ ($x = 0.3, 0.5, 0.7$)	Fe	Ni	Cr	Co	**Al_x**												[64]
$CoCrFeNi_2Mo_x$ ($x = 0, 0.25$)	Fe	Ni_2	Cr	Co			**Mo_x**										[81]
$AlCr_{1.5}CuFeNi_2Mn_x$ ($x = 0, 0.25, 0.5, 0.75, 1.0$)	Fe	Ni_2	$Cr_{1.5}$		Al			**Mn_x**	Cu								[99]
$AlCuCrFeMnW_x$ ($x = 0, 0.05, 0.1, 0.5, 1.0$)	Fe		Cr		Al			Mn	Cu					**W_x**			[100]
$CoCrFeNiMo_x$ ($x = 0.1, 0.2, 0.3, 0.4, 0.5$)	Fe	Ni	Cr	Co			**Mo_x**										[82]
$AlFeNiCoCuCr$	Fe	Ni	Cr	Co	Al				Cu								[69]
$Al_xCoCrFeNiTi_y$ ($x = 0.3, 0.6, 0.9$ and $y = 0, 0.5$)	Fe	Ni	Cr	Co	**Al_x**	**Ti_y**											[73]
$AlCrxFeNi_2Cu_{1.6}$ ($x = 0.5, 1.5, 2.5$)	Fe	Ni_2	**Cr_x**		Al				$Cu_{1.6}$								[102]
$Al_xCrFeMoV$ ($x = 0, 0.2, 0.6, 1.0$)	Fe		Cr		**Al_x**		Mo						V				[71]
$CoCrFeMnNb_xNi$ ($x = 0, 0.25$)	Fe	Ni	Cr	Co				Mn		**Nb_x**							[93]
$Al_{2-x}CoCrFeNiTi_x$ ($x = 0, 0.2, 0.5, 0.8, 1.0, 1.2$)	Fe	Ni	Cr	Co	**Al_{2-x}**	**Ti_x**											[75]
$MoNbFeCrV$	Fe		Cr				Mo			Nb			V				[105]
$MoNbFeCrTi$	Fe		Cr			Ti	Mo			Nb							[105]
$MoNbFeVTi$	Fe					Ti	Mo			Nb			V				[105]
$AlCoCrFeNiSi_{0.1}$	Fe	Ni	Cr	Co	Al						$Si_{0.1}$						[68]
$CoCrFeNiW_x$ ($x = 0, 0.2, 0.5$)	Fe	Ni	Cr	Co										**W_x**			[101]
$Co_xCrCuFeMnNi$ ($x = 0.5, 1.0, 1.5, 2.0$)	Fe	Ni	Cr	**Co_x**				Mn	Cu								[104]
$CoCrFeMnNi$	Fe	Ni	Cr	Co				Mn									[90]
$CoFeNiMnCr$	Fe	Ni	Cr	Co				Mn									[109]
$CrFeCoNiNb_x$ ($x = 0.2, 0.4, 0.6, 1.0$)	Fe	Ni	Cr	Co						**Nb_x**							[92]
$CoCrFeNiMo_x$ ($x = 0, 0.2, 0.5, 0.8, 1.0$)	Fe	Ni	Cr	Co			**Mo_x**										[83]
$FeCoCrNiMo_x$ ($x = 0, 0.1, 0.3, 0.6$)	Fe	Ni	Cr	Co			**Mo_x**										[2]
$Al_{0.6}CoFeNiCr_{0.4}$	Fe	Ni	$Cr_{0.4}$	Co	$Al_{0.6}$												[74]
$AlCoCrFeNiTi_x$ ($x = 0, 0.4, 0.8. 1.0$)	Fe	Ni	Cr	Co	Al	**Ti_x**											[77]
$Al_xCoCrFeNi$ ($x = 0.3, 0.5, 0.7$)	Fe	Ni	Cr	Co	**Al_x**												[65]
$AlCrFe_2Ni_2Mo_x$ ($x = 0, 0.05, 0.1, 0.15$)	Fe2	Ni2	Cr	Co	Al		**Mo_x**										[85]
$AlCoCrFeNi$	Fe	Ni	Cr	Co	Al												[67]
$AlCoCrFeNi_x$ ($x = 1.0, 1.4, 1.8$)	Fe	**Ni_x**	Cr	Co	Al												[106]
$FeNiCoCrCu$	Fe	Ni	Cr	Co					Cu								[89]
$FeNiCoCrMn$	Fe	Ni	Cr	Co				Mn									[89]
$Al_{0.3}Cr_xFeCoNi$ ($x = 0, 0.5, 1.0, 1.5, 1.7, 2.0$)	Fe	Ni	**Cr_x**	Co	$Al_{0.3}$												[103]

López Ríos et al. [106] investigated the effect of nickel on the corrosion behaviour of the $AlCoCrFeNi_x$ ($x = 1.0, 1.4, 1.8$ molar ratio) HEAs, in simulated biological medium (simulated body fluid) containing 1 wt% NaCl at 37 °C (for application in medical apparatus for surgery or implants). The higher the pitting potential value E_{pit}, the more resistant the alloy is to pitting corrosion. The pitting protection potential E_{pp} is determined when the current density declines drastically because of the repassivation of pits. $\Delta_{pit\text{-}pp}$ is the difference between pitting potential and pitting protection, which characterizes the tendency of repassivation of the pits. Larger $\Delta_{pit\text{-}pp}$ values indicate more stable pits on the passive layer. Among the three HEAs, $AlCrFeCoNi_{1.8}$ has the highest E_{pit} and the largest $\Delta_{pit\text{-}pp}$. Furthermore, the corrosion current densities of all the HEAs are much lower than that of the 304 stainless steel.

Table 3 summarizes the most common HEAs used for corrosion resistance described in Section 3.

4. Wear and corrosion (tribocorrosion) behaviour of HEAs

This section deals with the literature studying in the same work both the wear and corrosion behaviour of HEAs. In fact, tribocorrosion is defined as the science of a material degradation resulting from the interaction of mechanical loading and electrochemical reactions that occur between various elements of a tribosystem exposed to a corrosive environment. Published papers about the tribocorrosion of HEAs are scarce. Table 4 summarizes the composition of the HEAs studied from the tribocorrosion point of view, their preparation method, the wear-corrosion tests performed and some of the wear-corrosion parameters measured.

Kumar et al. [108] reported that the $Al_{0.1}CrFeCoNi$ HEA demonstrated a good general and pitting corrosion resistance compared to the 304 stainless steel in 3.5 wt% NaCl solution at room temperature. In another study, $Al_{0.1}CoCrFeNi$ is reported to be more wear resistant than the CoCrFeMnNi HEA in dry and marine environments [58]. Furthermore, the surface of $Al_{0.1}CrFeCoNi$ exhibits low corrosion rate, good resistance to passive layer breakdown and high degree of passivation, which indicates a better behaviour than CoCrFeMnNi. Therefore, $Al_{0.1}CoCrFeNi$ and its derivatives may attract significant scientific interest owing to their wear and corrosion resistance.

Nair et al. [110] evaluated the erosion-corrosion behaviour of the $Al_{0.1}CoCrFeNi$ HEA using a re-circulation type test rig. The experiments were performed in 3.5 wt% NaCl solution without sand particles (pure corrosion), and only with sand particles (pure erosion). Synergetic measurements were not performed in this study; electrochemical tests were carried out separately before and after the erosion tests. $Al_{0.1}CoCrFeNi$ has low hardness and yield strength; however, compared to the 316L stainless steel, it depicts high erosion-corrosion resistance, due to the formation of a stable passive layer, together with high polarization resistance, pitting resistance and decreased corrosion rates. $Al_{0.1}CoCrFeNi$ experiences minimum material loss due to erosion-corrosion at an oblique angle attack as well. Despite all that, an in-depth study is needed to investigate the simultaneous action of both erosion and corrosion with the help of specific equipment.

In the AlCoCrFeNi HEA, replacing Co with Ti gives rise to the new cobalt-free HEA AlCrFeNiTi; and if adding $x = 0.5$ molar ratio of Mn, its derivative $AlCrFeNiTiMn_x$ is obtained [111]. The wear resistance of those alloys decreases with the addition of manganese. The oxidation behaviour, evaluated as mass change per unit area as a function of the oxidation exposure time, was studied. The oxide growth rate of AlCrFeNiTi is lower than that of $AlCrFeNiTiMn_{0.5}$ which implies a better oxidation resistance of the former. And thus, the wear-oxidation resistance seems to be decreased for $AlCrFeNiTiMn_x$ HEAs. However, the simultaneous action of erosion and corrosion has yet to be investigated.

The $Ti_xZrNbTaMo$ ($x = 0.5, 1.0, 1.5, 2.0$ molar ratio) HEAs as implant materials, are easily affected by corrosion wear failure. Therefore, the development of new materials for biomedical implants with high corrosion and wear resistance has been the aim of many recent investigations [112]. Reducing the Ti content, the yield strength and the compressive strength increase significantly together with the microhardness. Also, $Ti_{0.5}ZrNbTaMo$ shows the best plastic deformation behaviour. The corrosion potential of the $Ti_xZrNbTaMo$ HEAs is lower than that of Ti_6Al_4V alloy, indicating the stability of the passive layer formed on the surface. Furthermore, $Ti_{0.5}ZrNbTaMo$ showed the lowest passivation current density. Therefore, these HEAs were confirmed to be corrosion resistant in phosphate-buffered saline (PBS) solution. This can be explained by the increase of tetravalent zirconium and molybdenum ion oxides (Zr^{4+}, Mo^{4+}), pentavalent niobium and tantalum ion oxides (Nb^{5+}, Ta^{5+}), as well as hexavalent molybdenum ion oxides Mo^{6+} due to the increase of oxygen when decreasing the Ti content. On the other hand, those HEAs exhibited superior wear resistance in both, wet and dry media due to the lower wear rate compared to Ti_6Al_4V alloy. The results also indicated lower coefficient of friction. Combining the electrochemical and the wear results, $Ti_{0.5}ZrNbTaMo$ demonstrates to be the most corrosive wear resistant among the four HEAs.

The MoNbTaTiZr HEA can be considered as an effective candidate to control the slurry erosion-corrosion [113]. The simultaneous corrosion-erosion phenomenon was investigated by using a slurry erosion test rig combined with a storage tank for the working media, as illustrated in Fig. 11. The hardness of MoNbTaTiZr is two times higher than that of the 316L stainless steel. Under slurry erosion-corrosion conditions, it showed 3.5 times higher resistance than the commercial alloy. The efficiency of the MoNbTaTiZr HEA is directly related to its high hardness, high polarization resistance of the passive film, low corrosion current density, and the absence of pitting corrosion signs. This was explained by the presence of TiO_2, ZrO_2, and Nb_2O_5 oxides which play an important role against corrosion.

Muangtong et al. [14] investigated the effect of the addition of tin in the CrFeCoNi HEA using corrosion and tribocorrosion techniques. When adding Sn, the microstructure exhibited a phase transition from ductile FCC single phase to dual phase containing FCC phase and Ni-Sn hard intermetallic phase. This transition allowed CrFeCoNiSn to show high polarization resistance in 0.6 M sodium chloride solution, and sufficient toughness against tribocorrosion due to a passive layer formed on the surface of the hard intermetallic phase.

The tribocorrosion properties of the additively manufactured CrFeCoNiMn HEA were investigated performing tribocorrosion tests on a reciprocating ball-on-flat tribometer coupled with a potentiostat in 3.5 wt% sodium chloride solution at room temperature [115].

Table 4
Summary of the investigations on corrosion-wear resistance.

Alloy composition	Alloy Preparation	Corrosion or oxidation conditions	Wear test conditions	Mass loss rate (mg/mm^2.h) related to erosion or material removal rate (mm^3/h)	Hardness (HV)	Coefficient of friction	Specific wear rate (mm^3/N/m)	Ref.
AlCrFeCoNiCu (comparison with 304 SS)	*Arc-melting → annealing for 5 h at the temperature of 600 and 1000 °C. *Polishing with 1000 grit SiC paper → degreasing in acetone → cleaning with alcohol → air drying	*Anodic polarization was measured in 3.5 wt % NaCl + 5 wt% sand particles having 80–120 μm at 500 rpm	Erosion: *Rotation velocity: 300, 500, 700 rpm *Impact angle: 90° *Erosion time: 3 h *Composition of the slurry pot: 10L aqueous solution of 5 wt% sand particles having 80–120 μm + 3.5% NaCl	Mass loss rate (10^{-3}): *At 500 rpm: 304SS: 4.6, HEA: 3.5, Annealed HEA at 600 °C: 2.4, Annealed HEA at 1000 °C: 3.5 *At 700 rpm: 304SS: 8.2, HEA: 5.9, Annealed HEA at 600 °C: 3.4, Annealed HEA at 1000 °C: 7	*304SS: 270 HV *HEA: 425 HV *Annealed HEA at 600 °C: 500 HV *Annealed HEA at 1000 °C: 380 HV	/	/	[114]
$Al_{0.1}$CoCrFeNi (comparison with 316 SS)	*Induction melting & hot isostatic pressing at 1200 °C and 100 MPa for 4 h → cooling to 343 °C for 3 h → cooling down to 191 °C for 1 h. *Polishing & grinding (down to 2000 grit size) → cleaning by acetone.	*Potentiodynamic polarization tests in PBS solution	Slurry Erosion: *Impact velocity: 20 m/s *Angle of impingement: 30° and 90° *Pure erosion experiment, samples were tested with cathodic protection to limit corrosion. *Slurry consists of sand particles 75–150 μm, mixed in 3.5 wt% NaCl solution.	Material removal rate: *For synergy erosion-corrosion, at oblique angle 30°: HEA: 0.39 316L: 0.75	*$Al_{0.1}$CoCrFeNi: 150 HV *316L SS: 226 HV	/	/	[110]
AlCrFeNiTi	*Arc melting *Polishing the cylindrical samples *Before OM and SEM, samples were etched in 2% HF + 3% HNO_3 + 95% H_2O	Oxidation test: Oxidation tests performed at 900 °C + holding for 100 h in a resistance furnace under air atmosphere → mass change per unit	Sliding wear: *Sliding load: 20 N *Sliding velocity: 0.8 m/s *Sliding distance: 1 Km *Medium: dry condition *Wear tests at room temperature under the dry sliding condition * GCrl5 counterpart	/	*AlCrFeNiTi: 616 HV *$AlCrFeNiTiMn_{0.5}$: 539.9 HV	*AlCrFeNiTi: 0.55 *$AlCrFeNiTiMn_{0.5}$: 0.55 with large fluctuations	*AlCrFeNiTi: 2.66 × 10^{-6} *$AlCrFeNiTiMn_{0.5}$: 5.10 × 10^{-6}	[111]
CrFeCoNiSn	*Compact arc melting (x5) *Grinding from P280 to P4000 in both sides →	Corrosion and tribocorrosion test: *0.6 M NaCl solution *Potential scan range: 0.7 to 1.3 for	Tribocorrosion: *Sliding load: 0.5 N *Sliding speed: 5 Hz *Sliding time: 3 h *stroke length: 2 mm	/	*CrFeCoNiSn: 516.90 HV *CrFeCoNi: 126.40 HV	*CrFeCoNi: 0.34/OCP *CrFeCoNiSn: 0.31/OCP	*CrFeCoNi: 7.57 × 10^{-6}/OCP *CrFeCoNiSn: 1.77 × 10^{-6}/OCP	[14]

(*continued on next page*)

Table 4 (*continued*)

Alloy composition	Alloy Preparation	Corrosion or oxidation conditions	Wear test conditions	Mass loss rate (mg/mm^2.h) related to erosion or material removal rate (mm^3/h)	Hardness (HV)	Coefficient of friction	Specific wear rate (mm^3/N/m)	Ref.
	polishing with 1 μm grain-size diamond suspension	CrFeCoNiSn, to 0.6 for CrFeCoNi *Scan rate: 5 mV/s	*Sliding distance: 216 m *Temperature: room *Alumina ball as a counterpart					
MoNbTaTiZr (comparison with 316 SS)	*Vacuum arc melting (x5) *Grinding– > polishing using sand papers down to 3000 grit size.	Slurry erosion-corrosion test: *3.5% NaCl solution at 37 °C *Experiments were performed in an open environment after 2 h of OCP stabilization	Slurry erosion: *Sliding velocity: 20 m/s *Sliding time: 2 h *Impingement angles: 30° and 90° *Slurry was prepared using river sand (75–150 μm), mixed with tap water (PH = 7.72)	Material removal rate: *Synergy erosion-corrosion, at oblique angle 30°: *MoNbTaTiZr: 0.22 *316L: 0.47 *Erosion at oblique angle 30°: *MoNbTaTiZr: 0.26 *316L: 0.89	*MoNbTaTiZr: 500 HV *316L: 275 HV	/	/	[113]
$Ti_xZrNbTaMo$ (x = 0.5, 1, 1.5, 2)	*Arc melting, *Grinding (up to 2000 grit size) → polishing with 2000 grit SiC sandpaper → ultrasonic cleaning in acetone, ethanol, and deionized water.	*The potentiodynamic polarization curves of the HEAs were examined in the phosphate buffered saline (PBS) solution: KCl: 0.20 g/L, NaCl: 8.01 g/L, KH_2PO_4: 0.20 g/L, Na_2HPO_4: 1.15 g/L *pH = 7.4–7.46	Reciprocating sliding wear: *Sliding load: 5 N *Sliding velocity: 60 r/min *Sliding time: 30 min *Si_3N_4 ball as a counterpart	/	x = 0.5: 490 HV x = 1: 482 HV x = 1.5: 450 HV x = 2: 432 HV	Ti_6Al_4V: 0.63 x = 0.5: 0.7 x = 1: 0.7 x = 1.5: 0.63 x = 2: 0.60	*Wet conditions: Ti_6Al_4V: 4.6×10^{-7} x = 0.5: 2.45×10^{-7} x = 1 : 2.27×10^{-7} x = 1.5: 1.85×10^{-7} x = 2: 1.52×10^{-7}	[112]
$AlCoCrFeNiTi_{0.5}$ AlCoCrFeNiCu	*Arc melting and re-melting at least four times. * Polished down to a 2000-grit paper, ultrasonically cleaned in acetone.	*Immersion tests: Samples were weighed, immersed in 90 wt% H_2O_2 solution, then removed after immersion for 7 days, 14 days and 28 days and reweighed.	Pin on disc: *$AlCoCrFeNiTi_{0.5}$ HEA/Si_3N_4 at 50 N and 0.69 m/s under H_2O_2 solution with different concentrations of 0 wt % (deionized water), 30 wt %, 60 wt% and 90 wt% *$AlCoCrFeNiTi_{0.5}$ and AlCoCrFeNiCu HEAs/Si_3N_4 ceramic under 50 N and 90 wt% H_2O_2 solution at the different sliding speeds of 0.69 m/s, 0.92 m/s, 1.15 m/s and 1.38 m/s	For $AlCoCrFeNiTi_{0.5}$ alloy after immersing 14 days is 0.00209 mm/a (millimeters per annum).	/	*Deionized water: $AlCoCrFeNiTi_{0.5}$ alloy COF ≈0.200. * 90 wt%: $AlCoCrFeNiTi_{0.5}$ alloy COF ≈0.015.	*Deionized water: $AlCoCrFeNiTi_{0.5}$ alloy wear loss ≈16.0 mg. * 90 wt%: $AlCoCrFeNiTi_{0.5}$ alloy wear loss ≈0.3 mg.	[116]

(*continued on next page*)

Table 4 (*continued*)

Alloy composition	Alloy Preparation	Corrosion or oxidation conditions	Wear test conditions	Mass loss rate (mg/mm^2.h) related to erosion or material removal rate (mm^3/h)	Hardness (HV)	Coefficient of friction	Specific wear rate (mm^3/N/m)	Ref.
$Al_{0.07}Co_{1.26}Cr_{1.80}Fe_{1.42}Mn_{1.35}Ni_{1.10}$	*Vacuum arc melting, re-melted and solidified 5 times and flipped before each re-melting operation. * Ground with 320–1200 grit SiC papers, washed with distilled water and sonicated in methanol for 10 min. *Boronized for 4 h at temperatures of 900, 950, and 1000 °C.	Tribocorrosion in ambient air, 3.5% NaCl and 5% H_2SO_4.	Duration of all the wear tests is 1800 s. Ball on disc against WC ball, normal load of 20 N, a sliding distance of 250 m and sliding velocity of 0.15 m/s.	As-cast HEA: *ambient air: 62.27×10^{-8} mm^3 *3.5% NaCl: 47.27×10^{-8} mm^3 *5% H_2SO_4: 77.84×10^{-8} mm^3 Sample 1000–4: *ambient air: 23.11×10^{-9} mm^3 *3.5% NaCl: 16.26×10^{-9} mm^3 *5% H_2SO_4: 24.95×10^{-9} mm^3	Surface hardness: Boronization at 900 °C = 26.75 GPa Boronization at 950 °C = 27.24 GPa Boronization at 1000 °C = 29.37 GPa	/	/	[117]
FeCrNiCoM (M = Al, Mo)	*Electric-arc furnace under N_2 atmosphere. *Polished by 500#, 1000# and 2000# SiC sand paper.	Tribocorrosion tests according to the ASTM G119- 09 standard.		N/A	N/A			[118]

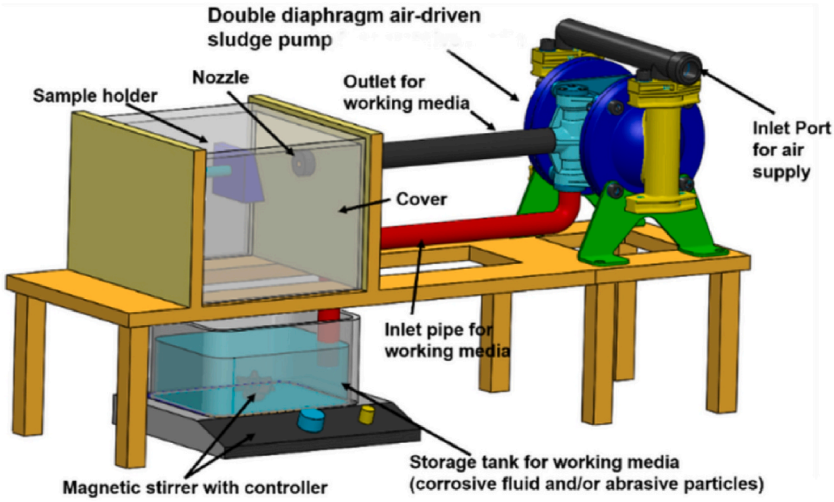

Fig. 11. Schematic illustrating the slurry erosion test rig used for tribocorrosion tests. Reproduced with permission from in Ref. [59].

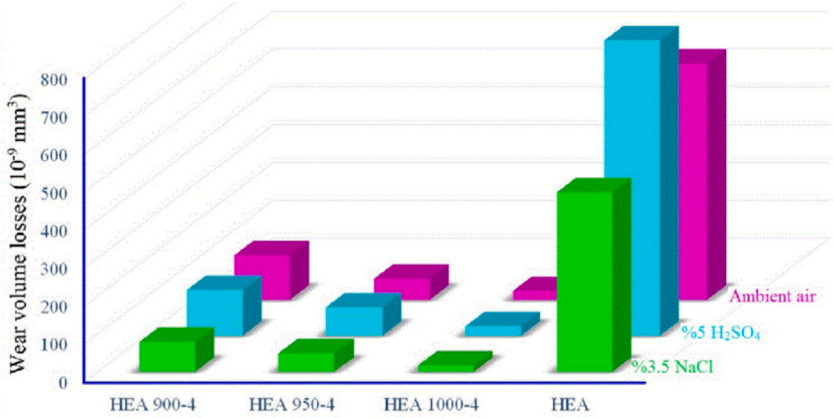

Fig. 12. Volumetric wear losses of the as-cast HEA and the boronized samples. Reproduced with permission from [117].

The experiments used the as-cast CrFeCoNiMn HEA produced by the conventional method (arc melting) as a counterpart. A big difference was detected when comparing the wear parameters (wear loss and wear rate) of the additively manufactured alloy and its equivalent as-cast HEA. As the load increased, the former showed excellent wear resistance. Furthermore, when using Al_2O_3 ball as a counterpart a superior tribocorrosion performance of the additively manufactured CoCrFeMnNi HEA was observed. This fact can be due to the refined microstructure and the improved passivation film formed during the additive manufacturing. Therefore, it can be concluded that the additive manufacturing method enhances the wear resistance and tribocorrosion performance compared to the conventional methods of production, such as arc melting.

After measuring the corrosion and erosion simultaneously using a slurry pot erosion tester equipped with an electrochemical system, Zhao et al. [114] reported that the annealing treatment can improve the erosion-corrosion resistance of the AlCrFeCoNiCu HEA. At 600 °C, this alloy showed the best erosion-corrosion resistance because of the precipitation of intermediate phases which have high hardness. At 1000 °C, the HEA had high corrosion resistance due to the decomposition of the BCC phase leading to a re-arranged crystalline structure. This decomposition affected the typical dendritic and interdendritic structures. Compared to the 304 stainless steel, AlCrFeCoNiCu has lower wear rate, and thus improved wear resistance.

Yu et al. [116] also investigated the corrosion and wear behaviour of the HEA AlCrFeCoNiCu together with the $AlCrFeCoNiTi_{0.5}$ HEA in 90 wt% H_2O_2 solution. They reported a low corrosion rate of 0.00209 mm/a for the $AlCoCrFeNiTi_{0.5}$ alloy after immersion during 14 days. It is deduced that the tribochemical reactions of the HEA/Si_3N_4 pair could hinder the mechanical wear. Additionally, the tribological properties are improved with the increase of the concentration of the H_2O_2 solution.

The fact that the HEAs often contain elements such as Fe, Co, Ni, that can form stable borides implies that boronizing may be a suitable surface modification method for HEAs in order to improve their properties. Karakaş et al. [117] evaluated the tribocorrosion behaviour of the boronized $Al_{0.07}Co_{1.26}Cr_{1.80}Fe_{1.42}Mn_{1.35}Ni_{1.10}$. The boronization process creates hard, protective metal borides on the surface of the alloys, reducing like that the surface damage during wear, and therefore, reducing the wear volume losses regardless of

the wear environment, as shown in Fig. 12.

Recently, Wang et al. [118] evaluated the corrosion, wear and synergism behaviors between them of the HEAs FeCrNiCo, FeCrNiCoAl and FeCrNiCoMo in artificial seawater. The importance of the synergism was assessed by the fact that the corrosion rate increase due to the wear was 100 times larger than the wear rate increase due to the corrosion.

5. Summary and outlook

The aim of this review was to highlight the most relevant studies undertaken since 2004, over almost 20 years, in wear, corrosion and wear-corrosion resistance in order to help designing and developing new HEAs. In this work we provided a comprehensive overview of the corrosion and wear resistance of HEAs to shed light on their uniqueness compared to conventional alloys, when responding to the modification of the study parameters, such as, content of base alloying elements (Al, Ti, Si, B …), temperature, heat treatment, sliding parameters (load, velocity, duration, distance). Furthermore, mechanisms, the relationship between microstructure and wear resistance, and between microstructure and corrosion resistance were described. The few articles that have been reported in the literature dealing with tribocorrosion (abrasion/erosion-corrosion) of HEAs have also been reviewed.

Despite the lack of the necessary information about their corrosion-wear synergy, numerous high entropy alloys were reported in the past few years due to their wear (erosion and abrasion) and corrosion properties, which make them preferable over a wide range of commercial alloys. The main wear and corrosion characteristics of these promising materials are summarized below:

- Among several compositions (x = 0, 0.3, 0.6, 0.9, 1.2 molar ratio), $C_{0.6}$CrFeCoNiMn HEA is considered as the optimal composition for higher wear resistance.
- Heat treatments (remelting, cold rolling, annealing) were found to be highly significant in improving the wear resistance of HEAs.
- In general, the tribological properties (frictional sliding and wear resistance) are dependent on temperature.
- In general, the erosion rate decreases with the increase of the impact angle, and the tribological properties of HEAs are highly dependent on the environment.
- It is difficult to extract conclusions about the influence of a certain chemical element on the behaviour of a HEA, since this influence depends on the rest of the elements composing the alloy. Alloying elements such as Al, Ti, Mo, Nb contribute differently in different HEAs. An element can enhance or reduce the corrosion resistance based on several parameters depending on the nature of the other elements, the amount of added element, the working environment (marine, basic, acid …) and its concentration. There is no obvious rule of thumb to determine whether a component improves corrosion resistance.
- As mentioned, HEAs are good candidates to substitute the already existing commercial alloys for applications involving wear and corrosion. Therefore, it is appropriate to define as potential applications for HEAs the applications that up to now have been covered by the conventional alloys, i.e., the fabrication of dies and moulds, cutting tools, car motors, high-temperature structural components, oil pipelines, sulfuric and phosphoric acid pumps, etc. Even more, HEAs offer the possibility to increase the lifespan of all those components in comparison with the use of standard commercial alloys.

Since there are several research articles on the corrosion resistance of HEAs, and few articles dealing with the wear resistance of HEAs, the part dealing with the synergy of both seems to be a challenging and important topic for further investigations. In fact, scarce studies are dealing with the simultaneous investigation of wear and corrosion, whereas other studies show a unique focus on a specific HEA studying its corrosion and wear behaviour separately and no connection is found between both properties. However, for the real-time assessment of wear and corrosion simultaneously, the synergetic effect evaluation using specific equipment is highly recommended.

Furthermore, the nature of the literature on wear resistance (erosion/abrasion) of HEAs, the complexity of wear mechanisms and the lack of relevant articles on wear-corrosion synergy create several challenges for scientists who are interested in considering the tribocorrosion of newly designed and developed HEAs. It is therefore concluded that the wear-corrosion synergy of HEAs is still largely unexplored; this new virgin field awaits exploration by more researchers. Due to their particular design approach and specific properties, it is expected that future HEAs will have compositions other than those listed in this review. The main constraint regarding the future development of HEAs for wear-corrosion applications is the lack of fundamental knowledge of their governing physical metallurgy principles. HEAs and conventional alloys share the same fabrication methods and characterization techniques. Also, both types of alloys can be modelled using the same computational methods. The main limitation concerning HEAs is the existing lack of knowledge regarding their physical metallurgy and therefore more fundamental studies are needed. More experimental data together with clear mechanisms and theories are required for HEAs in the future.

Data availability

No data was used for the research described in this article.

Ethics statement

Review and/or approval by an ethics committee was not needed for this study because this was a literature review and no new data were collected and analysed. For the same reason, informed consent was not required.

CRediT authorship contribution statement

Tarik Zirari: Writing – original draft, Conceptualization. **Vera Trabadelo:** Writing – review & editing, Supervision.

Declaration of competing interest

The authors declare that they have no known competing financial interests or personal relationships that could have appeared to influence the work reported in this paper.

Acknowledgements

The authors would like to thank the OCP Foundation for the financial support through the doctoral program from Mohammed VI Polytechnic University.

References

[1] S.J. Zinkle, G.S. Was, Materials challenges in nuclear energy, Acta Mater. 61 (3) (Feb. 2013) 735–758, https://doi.org/10.1016/j.actamat.2012.11.004.
[2] C. Dai, T. Zhao, C. Du, Z. Liu, D. Zhang, Effect of molybdenum content on the microstructure and corrosion behavior of FeCoCrNiMox high-entropy alloys, J. Mater. Sci. Technol. 46 (Jun. 2020) 64–73, https://doi.org/10.1016/j.jmst.2019.10.020.
[3] P. Muangtong, A. Rodchanarowan, D. Chaysuwan, N. Chanlek, R. Goodall, The corrosion behaviour of CoCrFeNi-x (x= Cu, Al, Sn) high entropy alloy systems in chloride solution, Corrosion Sci. 172 (Aug. 2020) 108740, https://doi.org/10.1016/j.corsci.2020.108740.
[4] J. Wu, Y. Chen, H. Zhu, A review on the tribological performances of High-Entropy Alloys, Adv. Eng. Mater. (Feb. 2022) 2101548, https://doi.org/10.1002/adem.202101548.
[5] M. Maher, I. Iraola-Arregui, H. Ben Youcef, B. Rhouta, V. Trabadelo, The synergistic effect of wear-corrosion in stainless steels: a review, Mater. Today: Proc. 51 (2022) 1975–1990, https://doi.org/10.1016/j.matpr.2021.05.010.
[6] J.R. Davis (Ed.), Surface Engineering for Corrosion and Wear Resistance, ASM International : Institute of Materials, Materials Park, OH, 2001.
[7] G.T. Burstein, K. Sasaki, Effect of impact angle on the slurry erosion–corrosion of 304L stainless steel, Wear 240 (1–2) (May 2000) 80–94, https://doi.org/10.1016/S0043-1648(00)00344-6.
[8] H. Zhou, Q. Ji, W. Liu, H. Ma, Y. Lei, K. Zhu, Experimental study on erosion-corrosion behavior of liquid–solid swirling flow in pipeline, Mater. Des. 214 (Feb. 2022) 110376, https://doi.org/10.1016/j.matdes.2021.110376.
[9] A. Ayyagari, V. Hasannaeimi, H. Grewal, H. Arora, S. Mukherjee, Corrosion, erosion and wear behavior of complex concentrated alloys: a review, Metals 8 (8) (Aug. 2018) 603, https://doi.org/10.3390/met8080603.
[10] M. Aliofkhazraei, Corrosion Inhibitors, Principles and Recent Applications, IntechOpen, Rijeka, 2018, https://doi.org/10.5772/intechopen.70101.
[11] W.D. Callister, D.G. Rethwisch, Fundamentals of Materials Science and Engineering: an Integrated Approach, third ed., John Wiley & Sons, Hoboken, NJ, 2008.
[12] D. Toboła, W. Brostow, K. Czechowski, P. Rusek, Improvement of wear resistance of some cold working tool steels, Wear 382–383 (2017) 29–39, https://doi.org/10.1016/j.wear.2017.03.023.
[13] A.S. Chaus, M. Sahul, R. Moravčík, R. Sobota, Role of microstructural factor in wear resistance and cutting performance of high-speed steel end mills, Wear 474 (475) (Jun. 2021) 203865, https://doi.org/10.1016/j.wear.2021.203865.
[14] P. Muangtong, R.M. Namus, R. Goodall, Improved tribocorrosion resistance by addition of Sn to CrFeCoNi high entropy alloy, Metals 11 (1) (2020) 13, https://doi.org/10.3390/met11010013.
[15] D.B. Miracle, High entropy alloys as a bold step forward in alloy development, Nat. Commun. 10 (1) (2019) 1805, https://doi.org/10.1038/s41467-019-09700-1.
[16] C.B. Nascimento, U. Donatus, C.T. Ríos, M.C.L. de Oliveira, R.A. Antunes, A review on corrosion of High Entropy Alloys: exploring the interplay between corrosion properties, alloy composition, passive film stability and materials selection, Math. Res. 25 (2022) e20210442, https://doi.org/10.1590/1980-5373-mr-2021-0442.
[17] J.-W. Yeh, S.-K. Chen, S.-J. Lin, J.-Y. Gan, T.-S. Chin, T.-T. Shun, C.-H. Tsau, S.-Y. Chang, Nanostructured High-Entropy Alloys with multiple principal elements: novel alloy design concepts and outcomes, Adv. Eng. Mater. 6 (5) (2004) 299–303, https://doi.org/10.1002/adem.200300567.
[18] B. Cantor, I.T.H. Chang, P. Knight, A.J.B. Vincent, Microstructural development in equiatomic multicomponent alloys, Mater. Sci. Eng., A 375 (377) (Jul. 2004) 213–218, https://doi.org/10.1016/j.msea.2003.10.257.
[19] B. S. Murty, S. Ranganathan, and J.-W. & J. W. Y. & S. R. Yeh, 'High-Entropy Alloys', p. 322.
[20] M. C. Gao, J-W. Yeh, P. K. Liaw, Y. Zhang, High Entropy Alloys, Fundamentals and Applications, Springer, ISBN 978-3-319-27011-1 ISBN 978-3-319-27013-5 (eBook) doi 10.1007/978-3-319-27013-5.
[21] S. Mukherjee, Complex concentrated alloys (CCAs)—current understanding and future opportunities, Metals 10 (9) (2020) 1253, https://doi.org/10.3390/met10091253.
[22] S. Gorsse, J.-P. Couzinié, D.B. Miracle, From high-entropy alloys to complex concentrated alloys, Compt. Rendus Phys. 19 (8) (Dec. 2018) 721–736, https://doi.org/10.1016/j.crhy.2018.09.004.
[23] C.-Y. Hsu, J.-W. Yeh, S.-K. Chen, T.-T. Shun, Wear resistance and high-temperature compression strength of FCC CuCoNiCrAl$_{0.5}$Fe alloy with boron addition, Metall. Mater. Trans. 35 (5) (May 2004) 1465–1469, https://doi.org/10.1007/s11661-004-0254-x.
[24] C.-C. Juan, M.-H. Tsai, C.-W. Tsai, C.-M. Lin, W.-R. Wang, C.-C. Yang, S.-K. Chen, S.-J. Lin, J.-W. Yeh, Enhanced mechanical properties of HfMoTaTiZr and HfMoNbTaTiZr refractory high-entropy alloys, Intermetallics 62 (2015) 76–83, https://doi.org/10.1016/j.intermet.2015.03.013.
[25] Y. Xu, Y. Xiao, D. Yi, H. Liu, L. Wu, J. Wen, Corrosion behavior of Ti–Nb–Ta–Zr–Fe alloy for biomedical applications in Ringer's solution, Trans. Nonferrous Metals Soc. China 25 (8) (Aug. 2015) 2556–2563, https://doi.org/10.1016/S1003-6326(15)63875-4.
[26] C. Shang, E. Axinte, W. Ge, Z. Zhang, Y. Wang, High-entropy alloy coatings with excellent mechanical, corrosion resistance and magnetic properties prepared by mechanical alloying and hot-pressing sintering, Surface. Interfac. 9 (Dec. 2017) 36–43, https://doi.org/10.1016/j.surfin.2017.06.012.
[27] J.-M. Wu, S.-J. Lin, J.-W. Yeh, S.-K. Chen, Y.-S. Huang, H.-C. Chen, Adhesive wear behavior of Al$_x$CoCrCuFeNi high-entropy alloys as a function of aluminum content, Wear 261 (5–6) (Sep. 2006) 513–519, https://doi.org/10.1016/j.wear.2005.12.008.
[28] M.-H. Chuang, M.-H. Tsai, W.-R. Wang, S.-J. Lin, J.-W. Yeh, Microstructure and wear behavior of Al$_x$Co1.5CrFeNi1.5Ti$_y$ high-entropy alloys, Acta Mater. 59 (16) (Sep. 2011) 6308–6317, https://doi.org/10.1016/j.actamat.2011.06.041.
[29] B. Gwalani, A.V. Ayyagari, D. Choudhuri, T. Scharf, S. Mukherjee, M. Gibson, R. Banerjee, Microstructure and wear resistance of an intermetallic-based Al$_{0.25}$Ti$_{0.75}$CoCrFeNi high entropy alloy, Mater. Chem. Phys. 210 (May 2018) 197–206, https://doi.org/10.1016/j.matchemphys.2017.06.034.
[30] B. Jin, N. Zhang, F. Wang, Y. Zhang, D. Li, Phase evolution and wear mechanism of AlCoCrFeNiSi$_x$ high-entropy alloys produced by arc melting, Mater. Res. Express 5 (9) (Aug. 2018) 096505, https://doi.org/10.1088/2053-1591/aad52b.
[31] O. Samoilova, N. Shaburova, A. Ostovari Moghaddam, E. Trofimov, Al$_{0.25}$CoCrFeNiSi$_{0.6}$ high entropy alloy with high hardness and improved wear resistance, Mater. Lett. 328 (Dec. 2022) 133190, https://doi.org/10.1016/j.matlet.2022.133190.

[32] B. Jin, N. Zhang, Y. Zhang, D. Li, Microstructure, phase composition and wear resistance of low valence electron concentration Al_xCoCrFeNiSi high-entropy alloys prepared by vacuum arc melting, J. Iron Steel Res. Int. 28 (2) (Feb. 2021) 181–189, https://doi.org/10.1007/s42243-020-00398-w.

[33] B. Gwalani, T. Torgerson, S. Dasari, A. Jagetia, M.S.K.K.Y. Nartu, S. Gangireddy, M. Pole, T. Wang, T.W. Scharf, R. Banerjee, Influence of fine-scale B2 precipitation on dynamic compression and wear properties in hypo-eutectic $Al_{0.5}$CoCrFeNi high-entropy alloy, J. Alloys Compd. 853 (Feb. 2021) 157126, https://doi.org/10.1016/j.jallcom.2020.157126.

[34] M. Löbel, T. Lindner, T. Mehner, T. Lampke, Influence of Titanium on microstructure, phase formation and wear behaviour of AlCoCrFeNiTi_x high-entropy alloy, Entropy 20 (7) (2018) 505, https://doi.org/10.3390/e20070505.

[35] Y. Lu, Y. Dong, S. Guo, L. Jiang, H. Kang, T. Wang, B. Wen, Z. Wang, J. Jie, Z. Cao, H. Ruan, T. Li, A promising new class of high-temperature alloys: eutectic High-Entropy Alloys, Sci. Rep. 4 (1) (May 2015) 6200, https://doi.org/10.1038/srep06200.

[36] W. Wang, S. Yuan, J. Chen, X. Li, Z. Niu, R. Wei, T. Wang, T. Zhang, S. Guan, F. Li, C. Chen, Corrosion in Cr-Fe-Co-Ni-Nb hypoeutectic and hypereutectic high entropy alloys, Mater. Today Commun. 31 (Jun. 2022) 103612, https://doi.org/10.1016/j.mtcomm.2022.103612.

[37] Y. Lu, H. Jiang, S. Guo, T. Wang, Z. Cao, T. Li, A new strategy to design eutectic high-entropy alloys using mixing enthalpy, Intermetallics 91 (Dec. 2017) 124–128, https://doi.org/10.1016/j.intermet.2017.09.001.

[38] X. Lin, M. Wang, G. Ren, D. Qiao, Y. Lu, T. Wang, T. Li, Microstructure evolution and mechanical properties of CrFeNi$_x$$V_{0.64}$$Ta_{0.36}$ eutectic high-entropy alloys, Mater. Char. 181 (Nov. 2021) 111449, https://doi.org/10.1016/j.matchar.2021.111449.

[39] M.-R. Chen, S.-J. Lin, J.-W. Yeh, M.-H. Chuang, S.-K. Chen, Y.-S. Huang, Effect of vanadium addition on the microstructure, hardness, and wear resistance of $Al_{0.5}$CoCrCuFeNi high-entropy alloy, Metall. Mater. Trans. 37 (5) (May 2006) 1363–1369, https://doi.org/10.1007/s11661-006-0081-3.

[40] C.-Y. Hsu, T.-S. Sheu, J.-W. Yeh, S.-K. Chen, Effect of iron content on wear behavior of AlCoCrFe$_x$$Mo_{0.5}$Ni high-entropy alloys, Wear 268 (5–6) (Feb. 2010) 653–659, https://doi.org/10.1016/j.wear.2009.10.013.

[41] J.-K. Xiao, H. Tan, J. Chen, A. Martini, C. Zhang, Effect of carbon content on microstructure, hardness and wear resistance of CoCrFeMnNiC_x high-entropy alloys, J. Alloys Compd. 847 (2020) 156533, https://doi.org/10.1016/j.jallcom.2020.156533.

[42] D. Kong, J. Guo, R. Liu, X. Zhang, Y. Song, Z. Li, F. Guo, X. Xing, Y. Xu, W. Wang, Effect of remelting and annealing on the wear resistance of AlCoCrFeNi$Ti_{0.5}$ high entropy alloys, Intermetallics 114 (2019) 106560, https://doi.org/10.1016/j.intermet.2019.106560.

[43] M. Chen, L. Lan, X. Shi, H. Yang, M. Zhang, J. Qiao, The tribological properties of $Al_{0.6}$CoCrFeNi high-entropy alloy with the σ phase precipitation at elevated temperature, J. Alloys Compd. 777 (Mar. 2019) 180–189, https://doi.org/10.1016/j.jallcom.2018.10.393.

[44] L.M. Du, L.W. Lan, S. Zhu, H.J. Yang, X.H. Shi, P.K. Liaw, J.W. Qiao, Effects of temperature on the tribological behavior of $Al_{0.25}$CoCrFeNi high-entropy alloy, J. Mater. Sci. Technol. 35 (5) (2019) 917–925, https://doi.org/10.1016/j.jmst.2018.11.023.

[45] D. Kong, W. Wang, T. Zhang, J. Guo, Effect of superheating on microstructure and wear resistance of $Al_{1.8}$CrCuFeNi$_2$ high-entropy alloy, Mater. Lett. 311 (Mar. 2022) 131613, https://doi.org/10.1016/j.matlet.2021.131613.

[46] C. Nguyen, A.K. Tieu, G. Deng, D. Wexler, B. Tran, T.D. Vo, Study of wear and friction properties of a Co-free CrFeNi$Al_{0.4}$$Ti_{0.2}$ high entropy alloy from 600 to 950°C, Tribol. Int. 169 (May 2022) 107453, https://doi.org/10.1016/j.triboint.2022.107453.

[47] W. Guo, J. Li, M. Qi, Y. Xu, H.R. Ezatpour, Effects of heat treatment on the microstructure, wear behavior and corrosion resistance of AlCoCrFeNiSi high-entropy alloy, Intermetallics 138 (Nov. 2021) 107324, https://doi.org/10.1016/j.intermet.2021.107324.

[48] M. Pole, M. Sadeghilaridjani, J. Shittu, A. Ayyagari, S. Mukherjee, High temperature wear behavior of refractory high entropy alloys based on 4-5-6 elemental palette, J. Alloys Compd. 843 (2020) 156004, https://doi.org/10.1016/j.jallcom.2020.156004.

[49] A. Verma, P. Tarate, A.C. Abhyankar, M.R. Mohape, D.S. Gowtam, V.P. Deshmukh, T. Shanmugasundaram, High temperature wear in CoCrFeNiCu$_x$ high entropy alloys: the role of Cu, Scripta Mater. 161 (Mar. 2019) 28–31, https://doi.org/10.1016/j.scriptamat.2018.10.007.

[50] J. Joseph, N. Haghdadi, K. Shamlaye, P. Hodgson, M. Barnett, D. Fabijanic, The sliding wear behaviour of CoCrFeMnNi and Al_xCoCrFeNi high entropy alloys at elevated temperatures, Wear 428–429 (2019) 32–44, https://doi.org/10.1016/j.wear.2019.03.002.

[51] H. Cheng, Y. Fang, J. Xu, C. Zhu, P. Dai, S. Xue, Tribological properties of nano/ultrafine-grained FeCoCrNiMnAl_x high-entropy alloys over a wide range of temperatures, J. Alloys Compd. 817 (2020) 153305, https://doi.org/10.1016/j.jallcom.2019.153305.

[52] S. Kumar, A. Patnaik, A.K. Pradhan, V. Kumar, Room temperature wear study of Al0.4 FeCrNiCox (x= 0, 0.25, 0.5, 1.0 mol) high-entropy alloys under oil lubricating conditions, J. Mater. Res. 34 (5) (Mar. 2019) 841–853, https://doi.org/10.1557/jmr.2018.499.

[53] S. Kumar, A. Patnaik, A.K. Pradhan, V. Kumar, Dry sliding wear behavior of Al0.4FeCrNiCox (x= 0, 0.25, 0.5, 1.0 mol) High-Entropy Alloys, Metallogr. Microstruct. Anal. 8 (4) (Aug. 2019) 545–557, https://doi.org/10.1007/s13632-019-00551-2.

[54] S.A. Firstov, V.F. Gorban, N.A. Krapivka, M.V. Karpets, A.D. Kostenko, Wear resistance of high-entropy alloys, Powder Metall. Met. Ceram. 56 (3–4) (Jul. 2017) 158–164, https://doi.org/10.1007/s11106-017-9882-8.

[55] G. Deng, A.K. Tieu, X. Lan, L. Su, L. Wang, Q. Zhu, H. Zhu, Effects of normal load and velocity on the dry sliding tribological behaviour of CoCrFeNiMo0.2 high entropy alloy, Tribol. Int. 144 (Apr. 2020) 106116, https://doi.org/10.1016/j.triboint.2019.106116.

[56] M. Chen, X.H. Shi, H. Yang, P.K. Liaw, M.C. Gao, J.A. Hawk, J. Qiao, Wear behavior of Al0.6CoCrFeNi high-entropy alloys: effect of environments, J. Mater. Res. 33 (19) (Oct. 2018) 3310–3320, https://doi.org/10.1557/jmr.2018.279.

[57] Y. Liu, S. Ma, M.C. Gao, C. Zhang, T. Zhang, H. Yang, Z. Wang, J. Qiao, Tribological properties of AlCrCuFeNi2 High-Entropy Alloy in different conditions, Metall. Mater. Trans. 47 (7) (Jul. 2016) 3312–3321, https://doi.org/10.1007/s11661-016-3396-8.

[58] A. Ayyagari, C. Barthelemy, B. Gwalani, R. Banerjee, T.W. Scharf, S. Mukherjee, Reciprocating sliding wear behavior of high entropy alloys in dry and marine environments, Mater. Chem. Phys. 210 (May 2018) 162–169, https://doi.org/10.1016/j.matchemphys.2017.07.031.

[59] R.B. Nair, K. Selvam, H.S. Arora, S. Mukherjee, H. Singh, H.S. Grewal, Slurry erosion behavior of high entropy alloys, Wear 386 (387) (Sep. 2017) 230–238, https://doi.org/10.1016/j.wear.2017.01.020.

[60] K. Lentzaris, A. Poulia, E. Georgatis, A.G. Lekatou, A.E. Karantzalis, Analysis of microstructure and sliding wear behavior of Co1.5CrFeNi1.5Ti0.5 High-Entropy Alloy, J. Mater. Eng. Perform. 27 (10) (Oct. 2018) 5177–5186, https://doi.org/10.1007/s11665-018-3374-y.

[61] C.P. Lee, C.C. Chang, Y.Y. Chen, J.W. Yeh, H.C. Shih, Effect of the aluminium content of AlxCrFe1.5MnNi0.5 high-entropy alloys on the corrosion behaviour in aqueous environments, Corrosion Sci. 50 (7) (Jul. 2008) 2053–2060, https://doi.org/10.1016/j.corsci.2008.04.011.

[62] C.P. Lee, Y.Y. Chen, C.Y. Hsu, J.W. Yeh, H.C. Shih, Enhancing pitting corrosion resistance of AlxCrFe1.5MnNi0.5 high-entropy alloys by anodic treatment in sulfuric acid, Thin Solid Films 517 (3) (Dec. 2008) 1301–1305, https://doi.org/10.1016/j.tsf.2008.06.014.

[63] Y. Shi, B. Yang, X. Xie, J. Brechtl, K.A. Dahmen, P.K. Liaw, Corrosion of AlCoCrFeNi high-entropy alloys: Al-content and potential scan-rate dependent pitting behavior, Corrosion Sci. 119 (May 2017) 33–45, https://doi.org/10.1016/j.corsci.2017.02.019.

[64] Y. Shi, L. Collins, R. Feng, C. Zhang, N. Balke, P.K. Liaw, B. Yang, Homogenization of Al CoCrFeNi high-entropy alloys with improved corrosion resistance, Corrosion Sci. 133 (Apr. 2018) 120–131, https://doi.org/10.1016/j.corsci.2018.01.030.

[65] Y. Shi, J. Mo, F.-Y. Zhang, B. Yang, P.K. Liaw, Y. Zhao, In-situ visualization of corrosion behavior of AlCoCrFeNi high-entropy alloys during electrochemical polarization, J. Alloys Compd. 844 (Dec. 2020) 156014, https://doi.org/10.1016/j.jallcom.2020.156014.

[66] R. Wang, K. Zhang, C. Davies, X. Wu, Evolution of microstructure, mechanical and corrosion properties of AlCoCrFeNi high-entropy alloy prepared by direct laser fabrication, J. Alloys Compd. 694 (Feb. 2017) 971–981, https://doi.org/10.1016/j.jallcom.2016.10.138.

[67] A. Parakh, M. Vaidya, N. Kumar, R. Chetty, B.S. Murty, Effect of crystal structure and grain size on corrosion properties of AlCoCrFeNi high entropy alloy, J. Alloys Compd. 863 (May 2021) 158056, https://doi.org/10.1016/j.jallcom.2020.158056.

[68] C. Xiang, Z.M. Zhang, H.M. Fu, E.-H. Han, H.F. Zhang, J.Q. Wang, Microstructure and corrosion behavior of AlCoCrFeNiSi0.1 high-entropy alloy, Intermetallics 114 (Nov. 2019) 106599, https://doi.org/10.1016/j.intermet.2019.106599.

[69] X. Zhang, J. Guo, X. Zhang, Y. Song, Z. Li, X. Xing, D. Kong, Influence of remelting and annealing treatment on corrosion resistance of AlFeNiCoCuCr high entropy alloy in 3.5% NaCl solution, J. Alloys Compd. 775 (Feb. 2019) 565–570, https://doi.org/10.1016/j.jallcom.2018.10.081.

[70] Y.Y. Chen, T. Duval, U.D. Hung, J.W. Yeh, H.C. Shih, Microstructure and electrochemical properties of high entropy alloys—a comparison with type-304 stainless steel, Corrosion Sci. 47 (9) (Sep. 2005) 2257–2279, https://doi.org/10.1016/j.corsci.2004.11.008.

[71] A. Raza, S. Abdulahad, B. Kang, H.J. Ryu, S.H. Hong, Corrosion resistance of weight reduced AlxCrFeMoV high entropy alloys, Appl. Surf. Sci. 485 (Aug. 2019) 368–374, https://doi.org/10.1016/j.apsusc.2019.03.173.

[72] J.J. Zhang, X.L. Yin, Y. Dong, Y.P. Lu, L. Jiang, T.M. Wang, T.J. Li, Corrosion properties of AlxCoCrFeNiTi0·5 high entropy alloys in 0.5M H2SO4 aqueous solution, Mater. Res. Innovat. 18 (sup4) (Jul. 2014), https://doi.org/10.1179/1432891714Z.000000000778. S4-756-S4-760.

[73] Y. Qiu, S. Thomas, D. Fabijanic, A.J. Barlow, H.L. Fraser, N. Birbilis, Microstructural evolution, electrochemical and corrosion properties of AlxCoCrFeNiTiy high entropy alloys, Mater. Des. 170 (May 2019) 107698, https://doi.org/10.1016/j.matdes.2019.107698.

[74] S. Wang, Y. Zhao, X. Xu, P. Cheng, H. Hou, Evolution of mechanical properties and corrosion resistance of Al0.6CoFeNiCr0.4 high-entropy alloys at different heat treatment temperature, Mater. Chem. Phys. 244 (Apr. 2020) 122700, https://doi.org/10.1016/j.matchemphys.2020.122700.

[75] Y. Zhao, M. Wang, H. Cui, Y. Zhao, X. Song, Y. Zeng, X. Gao, F. Lu, C. Wang, Q. Song, Effects of Ti-to-Al ratios on the phases, microstructures, mechanical properties, and corrosion resistance of Al2-xCoCrFeNiTix high-entropy alloys, J. Alloys Compd. 805 (Oct. 2019) 585–596, https://doi.org/10.1016/j.jallcom.2019.07.100.

[76] Z. Zhang, E. Axinte, W. Ge, C. Shang, Y. Wang, Microstructure, mechanical properties and corrosion resistance of CuZrY/Al, Ti, Hf series high-entropy alloys, Mater. Des. 108 (Oct. 2016) 106–113, https://doi.org/10.1016/j.matdes.2016.06.100.

[77] L. Huang, X.J. Wang, B.X. Huang, C.Z. Wang, Study on microstructure and corrosion resistance of AlCoCrFeNiTi(x) high-entropy alloys, IOP Conf. Ser. Mater. Sci. Eng. 774 (1) (Mar. 2020) 012058, https://doi.org/10.1088/1757-899X/774/1/012058.

[78] Z. Han, N. Chen, S. Lu, H. Luan, R. Peng, H. Xu, Y. Shao, Z. Peng, K. Yao, Structures and corrosion properties of the AlCrFeNiMo0.5Tix high entropy alloys, Mater. Corr. 69 (5) (May 2018) 641–647, https://doi.org/10.1002/maco.201709833.

[79] V. Kukshal, A. Patnaik, I.K. Bhat, Corrosion and thermal behaviour of AlCr1.5CuFeNi2Tix high-entropy alloys, Mater. Today: Proc. 5 (9) (2018) 17073–17079, https://doi.org/10.1016/j.matpr.2018.04.114.

[80] D.H. Xiao, P.F. Zhou, W.Q. Wu, H.Y. Diao, M.C. Gao, M. Song, P.K. Liaw, Microstructure, mechanical and corrosion behaviors of AlCoCuFeNi-(Cr,Ti) high entropy alloys, Mater. Des. 116 (Feb. 2017) 438–447, https://doi.org/10.1016/j.matdes.2016.12.036.

[81] A.A. Rodriguez, J.H. Tylczak, M.C. Gao, P.D. Jablonski, M. Detrois, M. Ziomek-Moroz, J.A. Hawk, Effect of Molybdenum on the corrosion behavior of High-Entropy Alloys CoCrFeNi2 and CoCrFeNi2Mo0.25 under sodium chloride aqueous conditions, Adv. Mater. Sci. Eng. 2018 (2018) 1–11, https://doi.org/10.1155/2018/3016304.

[82] X.-L. Shang, Z.-J. Wang, Q.-F. Wu, J.-C. Wang, J.-J. Li, J.-K. Yu, Effect of Mo addition on corrosion behavior of High-Entropy Alloys CoCrFeNiMox in aqueous environments, Acta Metall. Sin. 32 (1) (Jan. 2019) 41–51, https://doi.org/10.1007/s40195-018-0812-7.

[83] Z. Niu, Y. Wang, C. Geng, J. Xu, Y. Wang, Microstructural evolution, mechanical and corrosion behaviors of as-annealed CoCrFeNiMox (x = 0, 0.2, 0.5, 0.8, 1) high entropy alloys, J. Alloys Compd. 820 (Apr. 2020) 153273, https://doi.org/10.1016/j.jallcom.2019.153273.

[84] W. Jiao, H. Jiang, D. Qiao, J. He, H. Zhao, Y. Lu, T. Li, Effects of Mo on microstructure and mechanical properties of Fe2Ni2CrMox eutectic high entropy alloys, Mater. Chem. Phys. 260 (Feb. 2021) 124175, https://doi.org/10.1016/j.matchemphys.2020.124175.

[85] E.M. Godlewska, M. Mitoraj-Królikowska, J. Czerski, M. Jawańska, S. Gein, U. Hecht, Corrosion of Al(Co)CrFeNi high-entropy alloys, Front. Mater. 7 (Oct. 2020) 566336, https://doi.org/10.3389/fmats.2020.566336.

[86] Y.L. Chou, J.W. Yeh, H.C. Shih, The effect of molybdenum on the corrosion behaviour of the high-entropy alloys Co1.5CrFeNi1.5Ti0.5Mox in aqueous environments, Corrosion Sci. 52 (8) (Aug. 2010) 2571–2581, https://doi.org/10.1016/j.corsci.2010.04.004.

[87] Y.L. Chou, Y.C. Wang, J.W. Yeh, H.C. Shih, Pitting corrosion of the high-entropy alloy Co1.5CrFeNi1.5Ti0.5Mo0.1 in chloride-containing sulphate solutions, Corrosion Sci. 52 (10) (Oct. 2010) 3481–3491, https://doi.org/10.1016/j.corsci.2010.06.025.

[88] Y.-J. Hsu, W.-C. Chiang, J.-K. Wu, Corrosion behavior of FeCoNiCrCux high-entropy alloys in 3.5% sodium chloride solution, Mater. Chem. Phys. 92 (1) (Jul. 2005) 112–117, https://doi.org/10.1016/j.matchemphys.2005.01.001.

[89] S.A. Abolkassem, L.Z. Mohamed, G.A. Gaber, O.A. Elkady, Microstructure and corrosion behavior of FeNiCoCrCu and FeNiCoCrMn high entropy alloys manufactured by powder metallurgy in different acid media, J. Mater. Res. Technol. 10 (Jan. 2021) 1122–1142, https://doi.org/10.1016/j.jmrt.2020.12.016.

[90] H. Luo, S. Zou, Y.-H. Chen, Z. Li, C. Du, X. Li, Influence of carbon on the corrosion behaviour of interstitial equiatomic CoCrFeMnNi high-entropy alloys in a chlorinated concrete solution, Corrosion Sci. 163 (Feb. 2020) 108287, https://doi.org/10.1016/j.corsci.2019.108287.

[91] Z. Liu, J.M. Zeng, H.H. Zhan, Study on corrosion resistance of High-Entropy Alloys NiCoCrFeMnCuC in medium acid liquid, AMM 117–119 (Oct. 2011) 1816–1819, https://doi.org/10.4028/www.scientific.net/AMM.117-119.1816.

[92] C.-H. Tsau, C.-Y. Yeh, M.-C. Tsai, The effect of Nb-content on the microstructures and corrosion properties of CrFeCoNiNbx high-entropy alloys, Materials 12 (22) (Nov. 2019) 3716, https://doi.org/10.3390/ma12223716.

[93] D. Huang, J. Lu, Y. Zhuang, C. Tian, Y. Li, The role of Nb on the high temperature oxidation behavior of CoCrFeMnNbxNi high-entropy alloys, Corrosion Sci. 158 (Sep. 2019) 108088, https://doi.org/10.1016/j.corsci.2019.07.012.

[94] C.-H. Tsau, W.-L. Wang, Microstructures, hardness and corrosion behaviors of FeCoNiNb0.5Mo0.5 and FeCoNiNb High-Entropy Alloys, Materials 11 (1) (Dec. 2017) 16, https://doi.org/10.3390/ma11010016.

[95] S. Shuang, Z.Y. Ding, D. Chung, S.Q. Shi, Y. Yang, Corrosion resistant nanostructured eutectic high entropy alloy, Corrosion Sci. 164 (Mar. 2020) 108315, https://doi.org/10.1016/j.corsci.2019.108315.

[96] S. Shuang, Q. Yu, X. Gao, Q.F. He, J.Y. Zhang, S.Q. Shi, Y. Yang, Tuning the microstructure for superb corrosion resistance in eutectic high entropy alloy, J. Mater. Sci. Technol. 109 (May 2022) 197–208, https://doi.org/10.1016/j.jmst.2021.08.069.

[97] H.C. Shih, C.P. Lee, Y.Y. Chen, C.H. Wu, C.Y. Hsu, J.W. Yeh, Effect of boron on the corrosion properties of Al0.5CoCrCuFeNiBx high entropy alloys in 1N sulfuric acid, ECS Trans. 2 (26) (Dec. 2019) 15–33, https://doi.org/10.1149/1.2409020.

[98] Z.Y. Zheng, X.C. Li, C. Zhang, J.C. Li, Microstructure and corrosion behaviour of FeCoNiCuSnx high entropy alloys, Mater. Sci. Technol. 31 (10) (Jul. 2015) 1148–1152, https://doi.org/10.1179/1743284714Y.0000000730.

[99] V. Kukshal, A. Patnaik, I.K. Bhat, Effect of Mn on corrosion and thermal behaviour of AlCr1.5CuFeNi2Mnx high-entropy alloys, IOP Conf. Ser. Mater. Sci. Eng. 377 (Jun. 2018) 012023, https://doi.org/10.1088/1757-899X/377/1/012023.

[100] D. Kumar, O. Maulik, V.K. Sharma, Y.V.S.S. Prasad, V. Kumar, Understanding the effect of tungsten on corrosion behavior of AlCuCrFeMnWx high-entropy alloys in 3.5 wt.% NaCl solution, J. Mater. Eng. Perform. 27 (9) (Sep. 2018) 4481–4488, https://doi.org/10.1007/s11665-018-3536-y.

[101] Z. Niu, J. Xu, T. Wang, N. Wang, Z. Han, Y. Wang, Microstructure, mechanical properties and corrosion resistance of CoCrFeNiWx (x = 0, 0.2, 0.5) high entropy alloys, Intermetallics 112 (Sep. 2019) 106550, https://doi.org/10.1016/j.intermet.2019.106550.

[102] S. Yang, W. Yu, T. Liu, C. Li, Y. Zhang, Y. Qu, Effect of Cr content on corrosion behavior of AlCrxFeNi2Cu1.6 high entropy alloys, Mater. Res. Express 6 (7) (Apr. 2019) 076501, https://doi.org/10.1088/2053-1591/ab12ad.

[103] X. Yan, H. Guo, W. Yang, S. Pang, Q. Wang, Y. Liu, P.K. Liaw, T. Zhang, Al0.3CrxFeCoNi high-entropy alloys with high corrosion resistance and good mechanical properties, J. Alloys Compd. 860 (Apr. 2021) 158436, https://doi.org/10.1016/j.jallcom.2020.158436.

[104] R.-F. Zhao, B. Ren, B. Cai, Z.-X. Liu, G.-P. Zhang, J. Zhang, Corrosion behavior of CoxCrCuFeMnNi high-entropy alloys prepared by hot pressing sintered in 3.5% NaCl solution, Results Phys. 15 (Dec. 2019) 102667, https://doi.org/10.1016/j.rinp.2019.102667.

[105] C. Xiang, Z.-M. Zhang, H.-M. Fu, E.-H. Han, J.-Q. Wang, H.-F. Zhang, G.-D. Hu, Microstructure, mechanical properties, and corrosion behavior of MoNbFeCrV, MoNbFeCrTi, and MoNbFeVTi High-Entropy Alloys, Acta Metall. Sin. 32 (9) (Sep. 2019) 1053–1064, https://doi.org/10.1007/s40195-019-00935-x.

[106] M. López Ríos, P.P. Socorro Perdomo, I. Voiculescu, V. Geanta, V. Crăciun, I. Boerasu, J.C. Mirza Rosca, Effects of nickel content on the microstructure, microhardness and corrosion behavior of high-entropy AlCoCrFeNix alloys, Sci. Rep. 10 (1) (Dec. 2020) 21119, https://doi.org/10.1038/s41598-020-78108-5.

[107] X.-W. Qiu, Y.-P. Zhang, L. He, C. Liu, Microstructure and corrosion resistance of AlCrFeCuCo high entropy alloy, J. Alloys Compd. 549 (Feb. 2013) 195–199, https://doi.org/10.1016/j.jallcom.2012.09.091.

[108] N. Kumar, M. Fusco, M. Komarasamy, R.S. Mishra, M. Bourham, K.L. Murty, Understanding effect of 3.5 wt.% NaCl on the corrosion of Al0.1CoCrFeNi high-entropy alloy, J. Nucl. Mater. 495 (Nov. 2017) 154–163, https://doi.org/10.1016/j.jnucmat.2017.08.015.

[109] J. Yang, J. Wu, C.Y. Zhang, S.D. Zhang, B.J. Yang, W. Emori, J.Q. Wang, Effects of Mn on the electrochemical corrosion and passivation behavior of CoFeNiMnCr high-entropy alloy system in H2SO4 solution, J. Alloys Compd. 819 (Apr. 2020) 152943, https://doi.org/10.1016/j.jallcom.2019.152943.
[110] R.B. Nair, H.S. Arora, A. Ayyagari, S. Mukherjee, H.S. Grewal, High Entropy Alloys: prospective materials for tribo-corrosion applications, Adv. Eng. Mater. 20 (6) (Jun. 2018) 1700946, https://doi.org/10.1002/adem.201700946.
[111] Z.-S. Nong, Y.-N. Lei, J.-C. Zhu, Wear and oxidation resistances of AlCrFeNiTi-based high entropy alloys, Intermetallics 101 (Oct. 2018) 144–151, https://doi.org/10.1016/j.intermet.2018.07.017.
[112] N. Hua, W. Wang, Q. Wang, Y. Ye, S. Lin, L. Zhang, Q. Guo, J. Brechtl, P.K. Liaw, Mechanical, corrosion, and wear properties of biomedical Ti–Zr–Nb–Ta–Mo high entropy alloys, J. Alloys Compd. 861 (Apr. 2021) 157997, https://doi.org/10.1016/j.jallcom.2020.157997.
[113] A.K. Sharma, G. Perumal, H.S. Arora, H.S. Grewal, Slurry erosion–corrosion resistance of MoNbTaTiZr high entropy alloy, J. Bio Tribo. Corros. 7 (3) (Sep. 2021) 94, https://doi.org/10.1007/s40735-021-00530-7.
[114] J.H. Zhao, X.L. Ji, Y.P. Shan, Y. Fu, Z. Yao, On the microstructure and erosion–corrosion resistance of AlCrFeCoNiCu high-entropy alloy via annealing treatment, Mater. Sci. Technol. 32 (12) (Aug. 2016) 1271–1275, https://doi.org/10.1080/02670836.2015.1116494.
[115] J. Shittu, M. Sadeghilaridjani, M. Pole, S. Muskeri, J. Ren, Y. Liu, I. Tahoun, H. Arora, W. Chen, N. Dahotre, S. Mukherjee, Tribo-corrosion response of additively manufactured high-entropy alloy, npj Mater. Degrad. 5 (1) (Dec. 2021) 31, https://doi.org/10.1038/s41529-021-00177-2.
[116] Y. Yu, J. Wang, J. Yang, Z. Qiao, H. Duan, J. Li, J. Li, W. Liu, Corrosive and tribological behaviors of AlCoCrFeNi-M high entropy alloys under 90 wt.% H2O2 solution, Tribol. Int. 131 (2019) 24–32, https://doi.org/10.1016/j.triboint.2018.10.012.
[117] M.S. Karakaş, A. Günen, C. Çarboğa, Y. Karaca, M. Demir, Y. Altınay, A. Erdoğan, Microstructure, some mechanical properties and tribocorrosion wear behavior of boronized Al0.07Co1.26Cr1.80Fe1.42Mn1.35Ni1.10 high entropy alloy, J. Alloys Compd. 886 (2021) 161222, https://doi.org/10.1016/j.jallcom.2021.161222.
[118] J. Wang, W. Wen, J. Cheng, L. Dai, S. Li, X. Zhang, Y. Yang, H. Li, X. Hou, B. Wu, J. Wu, Tribocorrosion behavior of high-entropy alloys FeCrNiCoM (M= Al, Mo) in artificial seawater, Corr. Sci. 218 (2023) 111165, https://doi.org/10.1016/j.corsci.2023.111165.